

CRITICAL BEHAVIOR OF HADRONIC FLUCTUATIONS AND THE EFFECT OF FINAL-STATE RANDOMIZATION

Rudolph C. Hwa¹ and Yuanfang Wu²
Institute of Theoretical Science and Department of Physics
University of Oregon, Eugene, OR 97403-5203

Abstract

The critical behaviors of quark-hadron phase transition are explored by use of the Ising model adapted for hadron production. Various measures involving the fluctuations of the produced hadrons in bins of various sizes are examined with the aim of quantifying the clustering properties that are universal features of all critical phenomena. Some of the measures involve wavelet analysis. Two of the measures are found to exhibit the canonical power-law behavior near the critical temperature. The effect of final-state randomization is studied by requiring the produced particles to take random walks in the transverse plane. It is demonstrated that for the measures considered the dependence on the randomization process is weak. Since temperature is not a directly measurable variable, the average hadronic density of a portion of each event is used as the control variable that is measurable. The event-to-event fluctuations are taken into account in the study of the dependence of the chosen measures on that control variable. Phenomenologically verifiable critical behaviors are found and are proposed for use as a signature of quark-hadron phase transition in relativistic heavy-ion collisions.

1 Introduction

If indeed quark-gluon plasma is to be produced in relativistic heavy-ion collisions at high energy, such as at BNL-RHIC, there must be a quark-hadron phase transition (PT) when the plasma becomes cool enough, at which point hadrons are created and subsequently detected. The properties of that PT have not been extensively investigated for a number of reasons. Theoretically, the physics is not perturbative, and the fluctuation of hadronic observables is beyond the scope of feasibility of lattice gauge calculations at present. Experimentally, there is the preoccupation with the conventional main-stream issues, such as the primordial signatures, hydrodynamical flow, interferometry, etc. The most serious obstruction, however, is the common belief, based mostly on an extrapolation from low-energy nuclear collisions, that a hadron gas surrounds the plasma and that the final-state interaction in that gas obliterates all features of the PT, leaving the hadrons with no significant memory of their

¹E-mail address: hwa@oregon.uoregon.edu

²Permanent Address: Institute of Particle Physics, Hua Zhong Normal University, Wuhan, China

birth to be registered at the detector. One of the aims of this paper is to investigate the type of hadronic signature that can survive the final-state interaction and thereby to dispel the myth that critical behavior of quark-hadron PT is not observable.

If we take statistical physics as a guide, then we should expect the critical phenomena related to quark-hadron PT to be a vibrant area of study. The familiar critical behaviors of conventional systems are, for example, $C \sim |T - T_c|^{-\alpha}$ for the heat capacity of a thermal system, or $\chi \sim |T - T_c|^{-\gamma}$ for the susceptibility of a magnetic system, where T_c is the critical temperature. Is there any similar behavior for a quark system in its transition to hadrons? Can we find an observable in heavy-ion collisions, call it μ , such that its behavior near the critical point is

$$\mu \sim |T - T_c|^{-\kappa} \quad ? \quad (1)$$

Will μ survive the randomization process in the hadron gas, if it exists? Since the temperature T is not directly observable in heavy-ion collisions, is the critical exponent κ measurable? If not, what is the nature of the critical behavior that is subject to experimental test? These are some of the questions that we shall address and find answers to.

Our investigation cannot be based on nonperturbative QCD, which is too difficult to implement in treating the problem posed. In the absence of a reliable dynamical framework that can substitute for QCD, we appeal to the lesson already learned in statistical physics in that the universal properties of the critical phenomena are independent of the details of the microscopic dynamics. Only dimension and symmetry are of most importance. In the Ginzburg-Landau theory a universal scaling behavior on multiplicity fluctuations was derived [1], and later verified experimentally in quantum optics at the threshold of lasing [2]. That being a mean-field analysis, a more elaborate investigation that involves the study of spatial fluctuations near the critical point was subsequently carried out in the framework of the Ising model [3]. The result confirms the average behavior found in [1], but the work goes beyond the mean-field approximation by examining the PT process on a 2D lattice in a way that can best simulate the hadronization process. In this paper we continue to adopt the same approach, the only one available short of QCD, to study the fluctuation of spatial patterns of hadronization during PT, and to investigate whether the measures chosen can survive the randomization process of final-state interaction.

Instead of working with factorial moments, which are the measures of choice in the study of intermittency [4], we shall consider elementary wavelet analysis [5] to enhance the effectiveness of describing clusters of all sizes. Furthermore, we shall go beyond intermittency and study the fluctuations of spatial patterns [6, 7]. A measure that is based on the wavelet coefficients will be investigated in our search for a description of the critical behavior.

Our physical picture of the heavy-ion collision process at high enough energy and nuclear masses for quark-gluon plasma to be formed is the conventional one. After formation, a cylinder of high temperature plasma that is created undergoes rapid longitudinal expansion and slower transverse expansion. The interior is at $T > T_c$ so the medium stays in the deconfined state during most part of the time evolution of the system. We assume that with two flavors the quark-hadron PT is second order and that it takes place on the surface of the cylinder where T is lowest, namely T_c or slightly below. Thus the geometry of the system undergoing PT is 2-dimensional. For a time interval of the order of 1 fm/c, which

is roughly the hadronization time for the formation of a hadron, we map a section of that cylindrical surface to a square lattice to be studied in the Ising model. Hadrons are not formed uniformly on the surface. At different time segments of the evolutionary history the spatial patterns of hadron formation are different. Their fluctuations are simulated by the changing configurations of the Ising lattice. It is on the basis of this mapping between the physical surface and the mathematical lattice that we pursue our extensive investigation of the 2D Ising model in this paper.

2 Hadron Density in the Ising Model

Our first task is to establish a quantitative connection between the hadrons produced in a heavy-ion collision and the spins on a 2D lattice in the Ising model, which we use to simulate a second-order PT. A number of intermediate steps are needed to make that connection; they have been discussed in Ref. [3], which we summarize here.

The basis of our approach is the Ginzburg-Landau (GL) theory of PT. On the one hand, there is the Ising system of spins that can implement the GL description through a simple dynamical model capable of generating microscopic fluctuations [8]. On the other hand, particle production in the form of photons is well described by the GL theory, when a laser is operated at the threshold of lasing [9]. Our prediction for the scaling behavior associated with hadron production in the GL formalism [1, 10] turns out to be verified experimentally by photon production in quantum optics [2]. Thus we shall assume that the relationship between the GL order parameter and the hadron density to be the same as that for the photon density in the laser problem which is rigorously known.

The GL free energy density is

$$\mathcal{F}[\phi] = a |\phi(z)|^2 + b |\phi(z)|^4 + c |\partial\phi/\partial z|^2 \quad , \quad (2)$$

where $\phi(z)$ is the order parameter for the spatial coordinate at z in a 2D space. The parameters a , b and c need not concern us here. $\phi(z)$ is the link between hadrons and Ising spins. On one hand, the hadron density, in analogy to the photon density, is

$$\rho(z) \propto |\phi(z)|^2 \quad , \quad (3)$$

while on the other hand $\phi(z)$ is the local mean magnetization field, i.e.,

$$\phi(z) = A_c^{-1/2} \sum_{j \in A_c} s_j \quad , \quad (4)$$

where the sum is over all lattice sites in a cell of area $A_c = \epsilon^2$. In the absence of external field the total magnetization m_L of the whole lattice may be either positive or negative. We define s_j to be positive if the spin is aligned along m_L . Thus if σ_j is the lattice spin having values ± 1 , so that $m_L = \sum_{j \in L^2} \sigma_j$, then we define

$$s_j = \text{sgn}(m_L) \sigma_j \quad , \quad (5)$$

where $\text{sgn}(m_L)$ stands for the sign of m_L . This change of sign when m_L changes sign is irrelevant to the connection between the GL theory and the Ising model; however, (5) is

important in establishing a connection between hadron multiplicity and Ising spin. When $T > T_c$, hadronization is inhibited, and $\phi(z)$ is near zero since the summation of spins in a cell in (4) tends to cancel the site spins in the disordered state. If it is nonzero due to fluctuations, hadrons can be formed, but we associate them only with $\phi(z) > 0$, as we would for the ordered state, $T < T_c$, where hadrons are formed more copiously. In order to relate different event of collision with different configurations of the Ising spins in a uniform way, we must associate hadron formation with spins aligned with m_L , i.e., $\sum_j s_j > 0$, not $\sum_j \sigma_j > 0$. To summarize, the hadron density in the i th cell is

$$\rho_i = \lambda \left| \sum_{j \in A_c(i)} s_j \right|^2 \Theta \left(\sum_j s_j \right) \quad , \quad (6)$$

where Θ is the Heavyside function. The factor λ in (6) relates the mathematical quantity on the right side defined on an Ising lattice to the physical quantity of the number of particles in a cell emitted from the surface of quark-gluon plasma formed in a heavy-ion collision. Since λ is an unknown parameter in our attempt to simulate quark-hadron PT by the Ising model, we shall vary λ and regard any results that are sensitively dependent on λ as unphysical.

In our Monte Carlo simulation of the Ising model we use the Wolff algorithm [9, 11] to calculate the spin configurations for a lattice of size $L = 256$, using the Hamiltonian

$$H = -J \sum_{\langle ij \rangle} \sigma_i \sigma_j \quad , \quad (7)$$

where the sum is over the nearest neighbors. We choose the size of a cell to be $\epsilon = 4$ so the maximum value of ρ/λ in the ordered phase is $(4^2)^2 = 256$. Thus λ would have to be quite small to render the multiplicity in a cell to be a reasonably small number. Near T_c we expect ρ to vanish in many cells. A bin of size δ consists of $N_c = (\delta/\epsilon)^2$ cells, and the whole lattice consists of $M = (L/\delta)^2$ bins. The average density, averaged over all cells i , bins k , and configurations e , is

$$\langle \rho \rangle = \frac{1}{\mathcal{N}} \sum_{e=1}^{\mathcal{N}} \frac{1}{M} \sum_{k=1}^M \frac{1}{N_c} \sum_{i=1}^{N_c} \rho_i \quad , \quad (8)$$

where \mathcal{N} is the number of simulated configurations. In the following the results obtained are for $\mathcal{N} = 10^4$.

The dependence of $\langle \rho \rangle$ on T is shown in Fig. 1. It is evident that a continuous PT occurs at T_c somewhere between 2.0 and 2.5 in units of J/k_B . The precise value of T_c has been determined in [3] by examining the scaling behavior of the normalized factorial moments F_q . It is found that F_q behaves as M^{φ_q} only at $T = 2.315$. Since the critical point is characterized by the formation of clusters of all sizes in a scale independent way, we identify the critical temperature at $T_c = 2.315$. Note that $\langle \rho \rangle$ does not vanish for $T > T_c$, contrary to the behavior of the average magnetization in the limit of vanishing external field. The difference is due to our definition of hadron density ρ in (6) as opposed to the average magnetization being $\langle m_L \rangle$. For heavy-ion collisions it is reasonable to expect that hadrons can be produced even at $T > T_c$, though at reduced rate, due to local fluctuations in quark density and interactions.

For the sake of visualization of the spatial pattern of hadrons formed at T_c , we show in Fig. 2 a particular configuration on the lattice simulated at T_c . Squares of various sizes denote proportionally the cell densities of hadrons. It is evident that clusters of all sizes are formed. That is the well-known phenomenon at PT. Here it is the hadron density in a cell that is shown, not just spin up or down in the Ising problem.

Now, in search for a behavior analogous to (1), we focus on the T dependence of $\langle\rho\rangle$ for $T \leq T_c$. In Fig. 3 we show $\langle\rho\rangle - \langle\rho_c\rangle$ vs $T_c - T$ in a log-log plot with λ set at 1, $\langle\rho_c\rangle$ being $\langle\rho\rangle$ at T_c . For the range of T examined, it is clear that there exists a power-law behavior

$$\langle\rho\rangle - \langle\rho_c\rangle \propto (T_c - T)^\eta \quad (9)$$

with

$$\eta = 1.67 \quad . \quad (10)$$

For comparison, the susceptibility of a magnetic system has a critical exponent of ~ 1.3 .

If the final-state interaction in the hadron gas exists for several fm/c, long compared to the typical time for resonance decay (~ 1 fm/c), the multiplicity of stable hadrons (in strong interaction) produced would remain unchanged during that phase, since a temperature of ~ 140 MeV is not high enough to cause further production of particles. Thus the average hadron density is insensitive to the final-state interaction. However, (9) is not what is usually regarded as critical behavior, for which the exponent in a formula such as (1) is negative. Our search for a suitable measure of critical behavior therefore continues.

3 Fluctuations of Hadron Density

Since the fluctuation in particle production is large near the critical point, as evidenced by Fig. 2, we next consider the fluctuation of ρ from the average $\langle\rho\rangle$. Let the average density in bin k of size δ be

$$\rho_k = \left(\frac{\epsilon}{\delta}\right)^2 \sum_{i=1}^{N_c} \rho_i \quad (11)$$

where the sum is over all cells in bin k , the total number of which is $N_c = (\delta/\epsilon)^2$. Near T_c , ρ_k fluctuates from bin to bin, especially for small δ . Let us consider the moments

$$A_q(M) = \left\langle \left(\frac{\rho_k}{\langle\rho\rangle} \right)^q \right\rangle = \frac{1}{\mathcal{N}M} \sum_{e,k} \left(\frac{\rho_k}{\langle\rho\rangle} \right)^q \quad (12)$$

where $\langle\rho\rangle$ is given in (8). By studying the ratio $\rho_k/\langle\rho\rangle$, we avoid the dependence on the unknown λ ; moreover, we have $A_q = 1$ at $q = 1$. A representation of the properties of A_q is given by

$$J(M) = \left. \frac{d}{dq} A_q \right|_{q=1} = \left\langle \frac{\rho_k}{\langle\rho\rangle} \ln \frac{\rho_k}{\langle\rho\rangle} \right\rangle \quad . \quad (13)$$

One can also study $q = 2$ and higher powers, but $J(M)$ is sufficient for our purpose here.

In Fig. 4 we show the result of our simulation on $J(M)$. If A_q had a power-law dependence on $M = (L/\delta)^2$, then $J(M)$ would depend linearly on $\ln M$. Evidently, Fig. 4 does not exhibit any linear dependence at any T . However, the behaviors at various $T \leq T_c$ are similar. The situation is reminiscent of the behavior of F_q in the GL theory [1], where strict scaling $F_q \propto M^{\varphi_q}$ is not valid, but $F_q \propto F_2^{\beta_q}$ is valid. Similarly, we can consider here the dependence of $J(M)$ on $J_c(M)$, where $J_c(M) = J(M, T = T_c)$. As can be seen from Fig. 5, the points for $T < T_c$ can be well fitted by straight lines. Let us therefore write

$$J(M, T) = \alpha(T) J_c(M) \quad . \quad (14)$$

This is the property of a generalized form of scaling [12, 13]

$$A_q(M, T) \propto g(M)^{\tau_q(T)} \quad , \quad (15)$$

where $g(M)$ is some function of M independent of T . It follows directly from (13) that

$$\alpha(T) = \tau'(T)/\tau'(T_c) \quad , \quad (16)$$

where $\tau'(T) \equiv d\tau_q(T)/dq|_{q=1}$. We do not pursue the study of the generalized scaling (15) here.

From the slopes of the straightline fits in Fig. 5, we can exhibit the T dependence of $\alpha(T)$, shown in Fig. 6. We display $\alpha(T)$ in log-log plot so as to explore the possibility of the critical behavior

$$\alpha(T) \propto (T_c - T)^{-\zeta} \quad . \quad (17)$$

We have no illusion that (17) could be valid in the limit $T \rightarrow T_c$, since $\alpha(T_c) = 1$, by definition. However, for a range of T below T_c , Fig. 6 does show an approximate linearity. The corresponding value of the critical exponent η is

$$\zeta = 1.88 \quad . \quad (18)$$

Since (17) is invalid in the immediate neighborhood of T_c , it cannot be taken seriously as the defining characteristics of quark-hadron PT. Instead of (17), we regard Fig. 6 as containing more information about the fluctuations of the hadron density near the critical point. How such a behavior can be checked experimentally will be discussed in a later section below.

4 Fluctuations in Clustering

In the previous section we have studied the fluctuation properties of hadron density from bin to bin for all events. Since the bin density ρ_b is an average of the cell densities in a bin, it is not sensitive to the fluctuations of the cell densities within a bin. Clustering being such a characteristic feature of critical behavior where clusters of all sizes can occur, we need to go beyond ρ_b to capture the fluctuations of multiplicities among neighboring cells within the same bin. To that end we shall work with multiplicities instead of densities of hadrons, not

only for calculating spatial fluctuations, but also for considering temporal fluctuations in a later section when randomization due to final-state interaction is taken up.

In terms of the cell density ρ_i defined in (6) the cell multiplicity n_i is simply $\epsilon^2 \rho_i$. Since λ in (6) is unspecified, let us absorb the factor ϵ^2 into λ , i.e. redefining $\epsilon^2 \lambda \rightarrow \lambda$, and write

$$n_i = I \left[\lambda \left| \sum_{j \in A_i} s_j \right|^2 \Theta \left(\sum_j s_j \right) \right] , \quad (19)$$

where $I[x]$ signifies the largest integer $\leq x$. Thus n_i is discrete, although λ is treated as a continuous parameter ≤ 1 . For every configuration simulated on the lattice we have a matrix $C(c_1, c_2)$ that gives the value of the cell multiplicity n_i at the cell position (c_1, c_2) in the 2D space, where c_i ranges from 1 to $\ell = L/\epsilon$; i.e., $C(c_1, c_2) = n_i [i = (c_1, c_2)]$. Figure 2 is a pictorial representation of a possible configuration whose numerical description would be a particular matrix $C(c_1, c_2)$.

Now, for every bin in that $\ell \times \ell$ space we consider a transform through a function ψ^H that has the following property. Divide a square bin into four quadrants: in the two diagonal quadrants $\psi^H = +1$, in the two off-diagonal quadrants $\psi^H = -1$. If we use x and y to denote the two orthogonal coordinates of the square bin, normalized to unit length on both sides, then the precise definition of $\psi^H(x, y)$ is

$$\begin{aligned} \psi^H(x, y) &= 1, & 0 \leq x < 1/2, & 0 \leq y < 1/2, \\ &= -1, & 1/2 \leq x < 1, & 0 \leq y < 1/2, \\ &= -1, & 0 \leq x < 1/2, & 1/2 \leq y < 1, \\ &= 1, & 1/2 \leq x < 1, & 1/2 \leq y < 1, \\ &= 0, & \text{elsewhere} & . \end{aligned} \quad (20)$$

This is essentially a 2D Haar wavelet [5], but any prior knowledge about wavelet analysis is not needed for our discussion here.

We label a specific bin in the $\ell \times \ell$ space of cells by a triplet (j, k_1, k_2) , where the bin size δ_j is

$$\delta_j = \ell 2^{-j} \quad (21)$$

and the location of the bin is specified by (k_1, k_2) , with k_i ranging from 0 to $2^j - 1$. Clearly, the total number of bins is 2^{2j} . Thus j gives the level of zooming, and (k_1, k_2) describes the shift at that level. The label j used here and in the following should not be confused with the symbol j for site position on the lattice in the equations from (4) to (7). We can now define our basic wavelet function in the ℓ^2 space

$$\psi_{j,k_1,k_2}(c_1, c_2) = \psi^H \left(\frac{c_1}{\delta_j} - k_1, \frac{c_2}{\delta_j} - k_2 \right) . \quad (22)$$

It vanishes everywhere except in the j th level bin located at (k_1, k_2) , and in that bin it can only be ± 1 depending on the quadrant that c_1 and c_2 fall into.

Using $\psi_{j,k_1,k_2}(c_1, c_2)$ we define the wavelet transform of a configuration of cell multiplicities

$$w_{j,k_1,k_2} = \sum_{c_1, c_2} \psi_{j,k_1,k_2}(c_1, c_2) C(c_1, c_2) \quad , \quad (23)$$

where the sum is over all cells. It is clear that if $C(c_1, c_2)$ is uniform in a bin (j, k_1, k_2) , then the wavelet coefficient for that bin, w_{j,k_1,k_2} , is zero, although the average density ρ_b for that bin is not. Thus w_{j,k_1,k_2} measures the fluctuation from the average in a specific way. By varying j we can learn a great deal about the landscape of $C(c_1, c_2)$.

To study the fluctuations of the clustering within each configuration, but averaging over all configurations, we investigate the scaling properties of the moments of the wavelet coefficients, w_{j,k_1,k_2} . The wavelet coefficients, being more sensitive to fluctuations than F_q , have a better chance of generating a discernible signature of clustering patterns formed near the critical point. To that end, we define for a fixed j , for which $M = 2^{2j}$,

$$B_q(M) = \left\langle \left(\frac{w_{j,k_1,k_2}}{\langle w \rangle} \right)^q \right\rangle, \quad (24)$$

where

$$\langle \dots \rangle = \frac{1}{\mathcal{N}} \sum_{e=1}^{\mathcal{N}} \frac{1}{M} \sum_{k_1, k_2=0}^{2^j-1} \dots \quad (25)$$

Furthermore, we have

$$K(M) = \left. \frac{d}{dq} B_q \right|_{q=1} = \left\langle \frac{w_{j,k_1,k_2}}{\langle w \rangle} \ln \frac{w_{j,k_1,k_2}}{\langle w \rangle} \right\rangle, \quad (26)$$

which is the quantity that we shall investigate. In studying the ratio $w_{j,k_1,k_2}/\langle w \rangle$, the effects of λ in (19) tend to cancel, but not completely because n_i is a discretized version of a noninteger quantity at each cell. Thus some dependence of $K(M)$ on λ is expected, a property that will be examined.

The erraticity analysis [6, 7] originally designed to describe the event-to-event fluctuations was done using factorial moments F_q . For the problem of PT it was found that the erraticity indices turn out to be very small (of order 10^{-3}) [12], smaller than what experimental data can probably resolve. What is proposed in (24)-(26) is not erraticity analysis, and is not aimed at studying the fluctuations from configuration-to-configuration. Instead, $B_q(M)$ and $K(M)$ are measures of the fluctuations from bin to bin that are averaged over all configurations.

In Fig. 7 we show $K(M)$ vs $\ln M$ for a number of values of $T \leq T_c$. The dependence on M is evidently far more severe than that of $J(M)$ at large M . Due to the fact that j must be an integer, we cannot study at smaller steps in M . The fluctuations in small bins are clearly very strong, and they do not vanish in large bins, lest $K(M)$ would approach zero, as $M \rightarrow 1$. It means that hadrons are formed in clusters of all sizes, roughly with as much empty space on the lattice (unhadronized quarks in real space) between the clusters as there are hadronized cells.

To facilitate a description of the T dependence of $K(M, T)$, we plot $K(M, T)$ vs $K_c(M) = K(M, T_c)$, varying M parametrically, as shown in Fig. 8. Despite our inability to add points corresponding to intermediate bin sizes, the linearity of the behavior is self-evident. The points can be well fitted by straight lines, yielding the form

$$K(M, T) = \beta_0(T) + \beta(T)K_c(M) \quad . \quad (27)$$

Thus we can extract the slope $\beta(T)$ that depends only on T , and not on the bin sizes. It therefore characterizes the intrinsic properties of the system under PT, and may be more general than the Ising model used to derive it.

Figures 7 and 8 show the results of the calculation where λ has been set to 1 in (19). We now decrease λ to see how $\beta(T)$ depends on λ . That is shown in Fig. 9. Considering the fact that λ has been varied over two orders of magnitude, the form of $\beta(T)$ is basically stable. If we fit the last three points by straight lines in accordance to the formula

$$\beta(T) \propto (T_c - T)^{-\kappa} \quad , \quad (28)$$

the value of κ varies weakly with λ , as shown in Fig. 10, except at $\lambda = 0.02$ and 0.03 for unimportant reasons having to do with the discretization of n_i . Hereafter we shall adopt $\lambda = 0.05$ as the representative value and set

$$\kappa = 2.2 \quad . \quad (29)$$

Although (28) is not valid as $T \rightarrow T_c$, since by definition $\beta(T_c) = 1$, its approximate validity in a narrow range of T nevertheless captures a behavior remarkably similar to the conventional critical behaviors of familiar thermal and magnetic observables.

Since $\alpha(T)$ and $\beta(T)$ look very similar in Figs. 6 and 9, it is sensible to relate them directly, using T only as an implicit variable. That is, we plot β against α , as in Fig. 11, where all of the five temperature points are shown. They correspond to the $\lambda = 0.05$ points of $\alpha(T)$ and $\beta(T)$ in Figs. 6 and 9. We see that there exists a linear relationship, as exhibited by the straightline fit

$$\beta = a + b\alpha \quad , \quad (30)$$

where $a = -0.0623$ and $b = 1.11$. It is particularly remarkable in view of the nonlinear behavior in Figs. 6 and 9. There has been no prior suspicion that such a relationship should exist, so the experimental verification of (30) would be of great interest.

One may wonder how (30) can be consistent with (17) and (28) that have different exponents. Indeed, if one examines the linear fits in the log-log plots in Figs. 6 and 9, the deviations from the straightlines are larger than the deviations of the points in Fig. 11 from the solid line in that figure. In other words, when discrepancies from best fits are taken into account, the linear behavior exhibited in Fig. 11 is a better fit of the dependence of β on α , which is especially significant in view of the full range of all five points being related.

In the discussion in connection with (17) and (28) we have emphasized the behaviors of α and β in the region where T is not in the immediate neighborhood of T_c . We now examine further the region where T is closer to T_c . In Fig. 12 we have plotted the curves for $K(M, T)$ vs $J(M, T)$ for $T \leq T_c$. The solid curve for $T = T_c$ is of particular significance

if the PT occurs only at T_c . It is evident that the curves for T close to T_c have very similar shapes. Thus it appears that by shifting those curves they can all be overlaid on a universal curve that coincides with the curve at T_c . Since shifting horizontally and vertically correspond to rescaling the horizontal and vertical variables, we have replotted the curves in a set of new variables that involve changes in scales. The result is shown in Fig. 13, where $K(T)(T/T_c)^2$ is plotted against $J(T)(T/T_c)^{-10}$, with M being varied implicitly. All the curves for $2.28 \leq T \leq T_c = 2.315$ overlap and form a “universal” curve. Such a scaling behavior involving a range of T may be of theoretical interest only at this point, since T is not measurable. Nevertheless, the existence of such a universal curve is suggestive of some property that is like the Kadanoff scaling, where a change in the size of spin blocks can lead to a shift of the effective temperature [15]. Of course, the quantities involved here are quite different, and the reason for the universality found here deserves further investigation.

5 Observable Consequences

The results that we have obtained so far from analyzing the data generated by the Ising model are the T dependences of $\langle \rho \rangle$, $\alpha(T)$ and $\beta(T)$. Such results have no direct phenomenological implications, since the temperature T is not a directly measurable quantity in heavy-ion collisions, let alone the precise value of T_c . Thus equations such as (9), (17) and (28) are primarily of theoretical interest. They are the results of a search for behaviors that resembles the conventional critical behaviors. Now we ask, given these theoretical hints, what observable consequences of PT can be suggested that are experimentally testable.

To proceed, it is necessary to recognize first the important aspects in which the realistic situation of quark-hadron PT in heavy-ion collisions is more complicated than what has been simulated on the Ising lattice. A lattice configuration generated by the Ising model can represent the hadronization pattern on the surface of the plasma cylinder for only the time duration of the hadronization time t_h , roughly 1 fm/c. As time proceeds, the pattern changes, just as the lattice configuration changes upon repeated simulation. Under the assumption that the plasma interior is hot, with $T > T_c$, phase transition occurs on the surface at $T \leq T_c$ over a period of time long compared to t_h . What needs to be analyzed in the heavy-ion experiment is the hadronization patterns separated from one another in time segments of about t_h long. While that may be hard to achieve in present experiments, one can approximate that by making p_T cuts in small Δp_T intervals, since one expects from hydrodynamical considerations that a correspondence between p_T and evolution time τ exists such that hadrons emitted early have higher p_T than those emitted later [14]. We proceed under the supposition that it is possible to obtain from the heavy-ion data collected at a fixed transverse energy E_T many samples consisting of portions of the events that correspond to the hadronic patterns in the η - ϕ space and are the realistic counterparts of the simulated hadronic configurations $C(c_1, c_2)$ on the Ising lattice.

In the Ising model we can adjust the temperature T and study the T dependences of various measures. In heavy-ion collisions that cannot be done. We then consider two possible scenarios. First, we assume that the quark-hadron PT occurs at T_c only, and no other T . Second, we consider the possibility that various conditions of hydrodynamical flow may lead to hadronization at various T below T_c at different points of time in the evolutionary history

of the plasma. Let us refer to these two scenarios as A and B, respectively.

In scenario A we give up the possibility of studying the T dependence of PT. Our analysis of the data generated on the lattice nevertheless can serve as a guide to the analysis that can be done on the heavy-ion data. Since $J_c(M)$ and $K_c(M)$ are both observable, their dependences on M in Figs. 4 and 7 can both be checked. Due to the absence of an absolute relationship between bin sizes on the lattice and those in the experiments, it is best to examine the dependence of K_c on J_c with M being parametrically varied. Such a dependence is already shown by the solid line in Fig. 12 and by Fig. 13. Clearly, such a behavior is independent of the definitions of bin sizes on the lattice or in the experiment, and is a definitive characterization of the fluctuations of hadronic clusters at PT. The verification of the relationship between K_c and J_c would imply that the hadrons detected are created by a quark-hadron PT at T_c .

In scenario B where quark-hadron PT can occur at a range of T , the problem is significantly more complicated and will be the subject of our discussion for the remainder of this section. Let us first define a sample to be a portion of an event obtained by certain cuts (such as by a narrow Δp_T cut discussed in the beginning of this section) so that a sample corresponds to a configuration simulated on the Ising lattice. We assume that a sample is the result of hadronization at a common T , which may differ from T_c . That T may vary from sample to sample. For every sample the average density $\bar{\rho}$ of the hadronic configuration can be determined experimentally and should correspond to the average density calculated on the lattice according to

$$\bar{\rho} = \frac{1}{M} \sum_{k=1}^M \frac{1}{N_c} \sum_{i=1}^{N_c} \rho_i \quad , \quad (31)$$

This $\bar{\rho}$ is not the same as the theoretical overall average density $\langle \rho \rangle$ defined in (8), since the latter is averaged over all configurations at the same T , whereas $\bar{\rho}$ refers to a specific configuration on the lattice or a specific sample in the experiment. Since $\bar{\rho}$ can vary from sample to sample (as they do from configuration to configuration on the lattice) even when all samples are at the same temperature, let us first examine the distribution $P(\bar{\rho}, T)$ of $\bar{\rho}$ at fixed T . We have calculated that distribution at three representative values of T with the result shown in Fig. 14. As T is decreased from T_c , the average density increases, as more hadrons are produced in a phase transition. The shapes of the distributions vary quite significantly as functions of T . On the lattice the cell densities are bounded by a maximum, according to (6), of $\rho_{i,\max} = 256\lambda = 12.8$ (for $\lambda = 0.05$). The normalization of $\bar{\rho}$ should not be taken seriously in phenomenology, since the density on a lattice cannot be rigorously related to the hadron density in an experiment. We should therefore regard $\bar{\rho}$ as having an arbitrary scale. Nonetheless, these distributions at fixed T are important evidences that the event-to-event (and therefore configuration-to-configuration) fluctuations are large even if all kinematical variables of the collision processes are fixed, and if the uncontrollable dynamical variable T at hadronization is held constant.

In view of the rather wide distributions in Fig. 14 (which are all normalized to 1), it is clear that any experimental measure categorized according to the observed $\bar{\rho}$ must involve a convolution over the unobserved T . Thus, for example, in studying $K(M)$ we should convert

its T dependence to $\bar{\rho}$ dependence by use of the formula

$$K(M, \bar{\rho}) = \int dT P(\bar{\rho}, T) Q(T) K(M, T) \quad , \quad (32)$$

where $Q(T)$ is the probability that the quark-hadron PT will take place at $T \leq T_c$.

We have no deep insight on what $Q(T)$ should be. It can depend on the thermodynamics and hydrodynamics of the heavy-ion collision problem. One would expect that PT should take place in the immediate neighborhood of T_c . We shall take an exponential form for $Q(T)$ as a working hypothesis. Since the calculations in Secs. 3 and 4 are done for the range of T between $T_c = 2.315$ and $T = 2.25$ and interesting critical behaviors have been found theoretically in that range, we shall proceed on the assumption that $Q(T)$ is important only in that range. Accordingly, we adopt the following form

$$Q(T) = q_0 \exp [-(T_c - T)/0.08], \quad 2.24 \leq T \leq 2.32, \quad (33)$$

and require that it is zero elsewhere. The normalization factor is $q_0 = [0.08(1 - e^{-1})]^{-1}$.

We now can redo the calculations on $J(M)$ and $K(M)$ as in Secs. 3 and 4 by use of the convolution as in (32) and present the results in terms of $\bar{\rho}$. We shall set $\lambda = 0.05$. In Fig. 15 we show $J(M, \bar{\rho})$ for various bins of values of $\bar{\rho}$. Note that the highest curve (in solid line) is for $3.75 < \bar{\rho} < 4.0$, for which we shall use $\bar{\rho}_0 = 3.88$ to denote that bin, a value that shall play the role of T_c in Fig. 3. At lower $\bar{\rho}$ the curve for $J(M)$ is lower; this fringe effect shall be ignored in the scaling analysis below. That is, we shall consider only $\bar{\rho} > \bar{\rho}_0$ in the following. The similarity of the curves suggest following the same procedure as in Sec. 3. Thus we define $J_0(M) = J(M, \bar{\rho} = \bar{\rho}_0)$, and examine $J(M, \bar{\rho})$ vs $J_0(M)$. The result is shown in Fig. 16. The linear behavior is remarkable. Defining the slope to be $\alpha(\bar{\rho})$, we show its $\bar{\rho}$ dependence in Fig. 17. A power-law behavior can be identified, as indicated by the straight line, yielding

$$\alpha(\bar{\rho}) \propto (\bar{\rho} - \bar{\rho}_0)^{-\bar{\zeta}}, \quad \bar{\zeta} = 0.97. \quad (34)$$

The same procedure can be applied to $K(M, \bar{\rho})$, as done in Figs. 18-20. With $K_0(M) = K(M, \bar{\rho}_0)$ the linearity of the lines in Fig. 19 is even better than that in Fig. 7. Again, defining the slope to be $\beta(\bar{\rho})$, we obtain from Fig. 20 the behavior

$$\beta(\bar{\rho}) \propto (\bar{\rho} - \bar{\rho}_0)^{-\bar{\kappa}}, \quad \bar{\kappa} = 0.97. \quad (35)$$

Evidently, the behavior of $\beta(\bar{\rho})$ is essentially identical to that of $\alpha(\bar{\rho})$. Equations (34) and (35) represent the closest that we can identify as the critical behavior of quark-hadron PT. This time all the quantities involved are experimentally measurable.

Finally, we can plot $\beta(\bar{\rho})$ vs $\alpha(\bar{\rho})$ with $\bar{\rho}$ being the parametric variable. All five points fall on a straight line in Fig. 21. The linear behavior can be well expressed by the amazing formula

$$\alpha(\bar{\rho}) = \beta(\bar{\rho}) \quad (36)$$

with unit slope. We have no explanation for the simplicity of (36). It would be highly significant if this behavior can be verified by experiment.

6 Effects of Randomization

What we have studied so far are the properties of the hadrons formed on the cylindrical surface, which is mapped onto the Ising lattice. The observed hadrons that reach the detector must traverse the space between the cylindrical surface and the detector. If a hadron gas surrounds the plasma cylinder, then a hadron formed on the surface must undergo final-state interactions with other hadrons before it can move as a free particle to the detector. Assuming no further particle production in this last phase, the hadrons can only shift their positions in the η - ϕ plane in a random way, since the hadron gas plays the role of random scatterers and can offer no organized forces on a traversing hadron.

We shall take into account this randomization process by requiring each hadron to take random walks on the lattice. The step size is the distance between neighboring cells, i.e., ϵ . If a cell has $n_i > 1$, then each particle in the cell takes steps that are independent of what other particles in the cell do. A particle has five possible positions in each random step, four neighboring cells plus the original cell for no transverse movement. Denoting the number of steps by ν , we consider ν ranging from 1 to 6, although it is generally believed that 3-4 steps are adequate to represent the effect of randomization by the interactions in a hadron gas.

In considering random walk we must focus on the whereabouts of the particles, so hadron density must be converted to particle number by a specific choice of λ . Although we have avoided that choice in Sec. 3, we have found in Sec. 4 that $\lambda = 0.05$ is an appropriate choice. Thus we use the same λ now in calculating the effect of random walk on $J(M, T)$ and then on $\alpha(T)$. Fig. 22(a) summarizes the effect for ν up to 4, where we stop to avoid overlap of the points on the figure at higher ν . The general shape of $\alpha(T)$ is unchanged. Quantitative dependence of the index ζ , defined in (17), on ν is shown in Fig. 22(b), exhibiting insensitivity to randomization.

The same analysis has been done for $K(M, T)$ and then $\beta(T)$ with the result shown in Fig. 23. In this case the effect of random walk is more pronounced, especially at low ν , but for $4 \leq \nu \leq 6$ the effect stabilizes. Although $\beta(T)$ suffers more change than $\alpha(T)$, the overall effect does not invalidate the usefulness of the measures that we have considered. We show in Fig. 24 the effect of ν steps of randomization on the dependence of β on α . Evidently, the general linear dependence is unaltered by the randomization process.

We shall not redo the above calculation for α and β as functions of $\bar{\rho}$, since the effect of randomization should be similar on the experimental $\alpha(\bar{\rho})$ and $\beta(\bar{\rho})$. If the experimental data can produce a figure such as Fig. 21, showing that $\beta(\bar{\rho})$ is essentially the same as $\alpha(\bar{\rho})$, we can conclude on the basis of the study considered here that the effect of randomization is not so severe as to render the whole approach ineffective. We infer that the measures $J(M)$ and $K(M)$ must not be very sensitive to the redistribution of particles in the transverse plane, since it is not the individual local property of a hadron but the *scaling* properties of clusters of hadrons over a wide range of bin sizes that the fluctuation measures have extracted.

7 Summary

Using the Ising model and defining hadrons on the lattice in accordance to the Ginsburg-Landau description of quark-hadron PT, we have found a number of interesting features

about the critical behavior. First of all, the average hadron density on the surface of the plasma cylinder for a time interval around the hadronization time of a hadron depends on the surface temperature according as

$$\langle \rho \rangle - \langle \rho_c \rangle \propto (T_c - T)^\eta \quad , \quad \eta = 1.67 \quad . \quad (37)$$

Then there are two quantities $\alpha(T)$ and $\beta(T)$, defined in (14) and (27), that behave as

$$\alpha(T) \propto (T_c - T)^{-\zeta} \quad , \quad \zeta = 1.88 \quad . \quad (38)$$

$$\beta(T) \propto (T_c - T)^{-\kappa} \quad , \quad \kappa = 2.2 \quad . \quad (39)$$

These are behaviors of theoretical interest, since T is not directly measurable. Nonetheless, (38) and (39) confirm that there exist measures in the hadronic variables that exhibit the canonical form of critical behaviors.

Since the average density $\bar{\rho}$ in a sample is measurable, we have shown how the critical behaviors can be reexpressed in terms of $\bar{\rho}$ as

$$\alpha(\bar{\rho}) \propto (\bar{\rho} - \bar{\rho}_0)^{-\bar{\zeta}} \quad , \quad \beta(\bar{\rho}) \propto (\bar{\rho} - \bar{\rho}_0)^{-\bar{\kappa}} \quad , \quad (40)$$

$$\bar{\zeta} = \bar{\kappa} = 0.97 \quad . \quad (41)$$

The equations in (40) are expressed in terms of observables and should be checked by experiments. Furthermore, the direct dependence of $\beta(\bar{\rho})$ on $\alpha(\bar{\rho})$ over a wider range of $\bar{\rho}$ can also be examined. If it turns out that they are related approximately by $\alpha(\bar{\rho}) \approx \beta(\bar{\rho})$, then that would be a less restrictive, yet nevertheless valid, experimental signature of the critical behavior of a quark-hadron PT.

Experimental study of $J(M)$ and $K(M)$, defined in (13) and (26), involves less analysis and thus are more reliable phenomenologically. If PT occurs at $T = T_c$ only, then $J_c(M)$ and $K_c(M)$ are directly measurable. The verification of K_c vs J_c , as shown by the solid line in Fig. 12, would strongly indicate the occurrence of a PT.

None of the phenomenology suggested above would mean anything realistic if the hadron gas in the final state erases all memory of the properties of phase transition before the particles reach the detector. We have studied the effect of the randomization due to hadron gas on our measures, and found that within the framework of our modeling none of them are seriously influenced by the randomization procedure so long as the number of random steps in the η - ϕ plane is not too large. Those measures involve the fluctuations from bin to bin of either the average density of hadrons or the wavelet coefficients of the spatial patterns, both of which are evidently insensitive to the randomization.

An important assumption is made in this work, namely: cuts in small Δp_T bins can be made to select small $\Delta \tau$ bins in real time that can exhibit the various hadronic configurations of a phase transition process. Based on the intuition gained in this work, we conjecture that the general features of our result are insensitive to the precise validity of this assumption, provided that Δp_T is small enough. Only by doing the appropriate analysis of the actual heavy-ion collision data can we assess the plausibility of this assumption and the feasibility of the whole program discussed here to extract the critical behavior of quark-hadron phase transition.

It should be noted finally that there are two aspects about the work presented here. One is about the theoretical understanding of the properties of the critical behavior at the quark-hadron PT. The other is the attempt to find the means to determine those properties experimentally. Even if the latter effort fails because of our incomplete understanding of the actual collision and hadronization process, the former will remain valid and stand ready for verification by better phenomenology to come. Our result on the insensitivity of our proposed measure to the final-state effects provides the encouragement to persist in this difficult but worthwhile quest.

Acknowledgment

We are grateful to Drs. Z. Cao and Y. Gao for helpful discussions and assistance. This work was supported in part by U.S. Department of Energy under Grant No. DE-FG03-96ER40972.

References

- [1] R. C. Hwa and M. T. Nazirov, Phys. Rev. Lett. **69**, 741 (1992)
- [2] M. R. Young, Y. Qu, S. Singh and R. C. Hwa, Optics Comm. **105**, 325 (1994).
- [3] Z. Cao, Y. Gao and R. C. Hwa, Z. Phys. C **72**, 661 (1996).
- [4] E. A. DeWolf, I. M. Dremin, and W. Kittel, Phys. Rep. **270**, 1 (1996).
- [5] I. Daubechies, *Ten lectures on wavelets* (SIAM, 1992); G. Kaiser, *A friendly guide to wavelets* (Birkhäuser, Boston, 1994).
- [6] R. C. Hwa, Acta Physica Polonica B**27**, 1789 (1996).
- [7] Z. Cao and R. C. Hwa, Phys. Rev. Lett. **75**, 1268 (1995); Phys. Rev. D **53**, 6608 (1996); *ibid* **54**, 6674 (1996) .
- [8] J. J. Binney, M. J. Dowrick, A. J. Fisher, and M. E. J. Newman, *The Theory of Critical Phenomena* (Clarendon Press, Oxford, 1992).
- [9] R. Graham and H. Haken, Z. Physik **213**, 420 (1968); **237**, 31 (1970); V. DeGiorgio and M. Scully, Phys. Rev. A**2**, 1170 (1970).
- [10] R. C. Hwa, Phys. Rev. D **47**, 2773 (1993).
- [11] U. Wolff, Phys. Rev. Lett. **62**, 361 (1989).
- [12] Z. Cao and R. C. Hwa, Phys. Rev. E **56**, 326 (1997).
- [13] Z. Cao and R. C. Hwa, hep-ph/9901256.
- [14] R. C. Hwa, in *Nuclear Matter in Different Phases and Transitions*, Proceedings of Workshop at Les Houches, France, April 1998 (Kluwer Academic Publ., 1999).
- [15] L. Kadanoff, Physica **2**, 263 (1966).

Figure Captions

- Fig. 1** Temperature dependence of the average hadron density in arbitrary scale.
- Fig. 2** A representative configuration of hadron production in η - ϕ plane as simulated on the Ising lattice of size $\ell \times \ell$, where $\ell = L/\epsilon$ is the number of cells along each dimension. The size of a square is proportional to the hadron density of a cell.
- Fig. 3** Temperature dependence of average density for $T \leq T_c$. η is the slope of the straightline fit.
- Fig. 4** The dependence of $J(M)$ on M for various values of T .
- Fig. 5** The dependence of $J(M)$ on $J_c(M)$ for various values of T , where $J_c(M) = J(M, T)$ at $T = T_c$.
- Fig. 6** Critical behavior of $\alpha(T)$, where $\alpha(T)$ is defined in (14). $-\zeta$ is the slope of the straight line.
- Fig. 7** The dependence of $K(M)$ on M for various values of T .
- Fig. 8** The dependence of $K(M)$ on $K_c(M)$ for various values of T , where $K_c(M) = K(M, T)$ at $T = T_c$.
- Fig. 9** The dependence of $\beta(T)$, defined in (27), on T for various values of λ . The slope of the straight line is $-\kappa = -2.2$.
- Fig. 10** The dependence of the critical exponent κ on λ .
- Fig. 11** The direct relationship between $\beta(T)$ and $\alpha(T)$, when T is varied.
- Fig. 12** The direct relationship between $K(M, T)$ and $J(M, T)$, when M is varied but T fixed.
- Fig. 13** Same as Fig. 12 but in rescaled variables.
- Fig. 14** The probability distribution of the average density $\bar{\rho}$ in a configuration for three fixed T , generated by 10^4 configurations at each T . The scale of $\bar{\rho}$ is arbitrary.
- Fig. 15** The dependence of $J(M, \bar{\rho})$ on M for various values of $\bar{\rho}$.
- Fig. 16** The dependence of $J(M, \bar{\rho})$ on $J_0(M)$ for various values of $\bar{\rho}$, where $J_0(M) = J(M, \bar{\rho})$ at $\bar{\rho} = \bar{\rho}_0$.
- Fig. 17** Critical behavior of $\alpha(\bar{\rho})$, where $\alpha(\bar{\rho})$ is the slope of a straightline fit in Fig. 16.
- Fig. 18** The dependence of $K(M, \bar{\rho})$ on M for various values of $\bar{\rho}$.
- Fig. 19** The dependence of $K(M, \bar{\rho})$ on $K_0(M)$ for various values of $\bar{\rho}$, where $K_0(M) = K(M, \bar{\rho})$ at $\bar{\rho} = \bar{\rho}_0$.

- Fig. 20** Critical behavior of $\beta(\bar{\rho})$, where $\beta(\bar{\rho})$ is the slope of a straightline fit in Fig. 19.
- Fig. 21** The direct relationship between $\beta(\bar{\rho})$ and $\alpha(\bar{\rho})$, when $\bar{\rho}$ is varied.
- Fig. 22** The effect of randomization on (a) $\alpha(T)$ and (b) ζ , where ν is the number of steps of random walk.
- Fig. 23** The effect of randomization on (a) $\beta(T)$ and (b) κ , where ν is the number of steps of random walk.
- Fig. 24** The effect of randomization on the relationship between $\beta(T)$ and $\alpha(T)$.

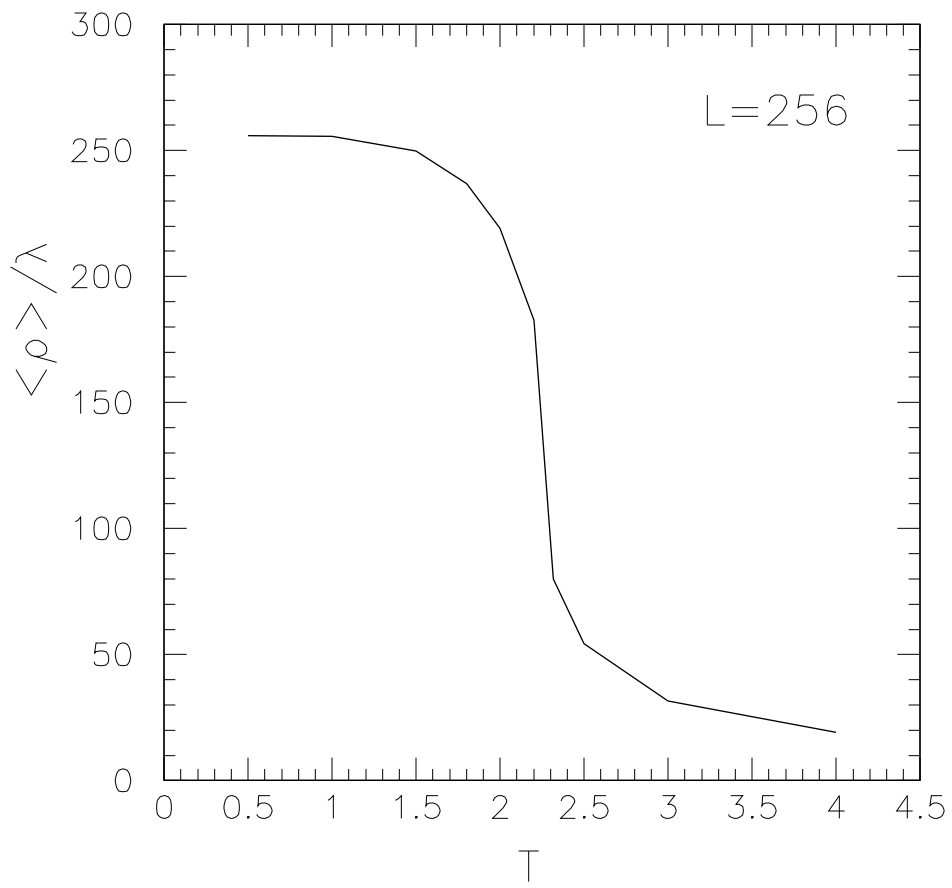


Fig. 1

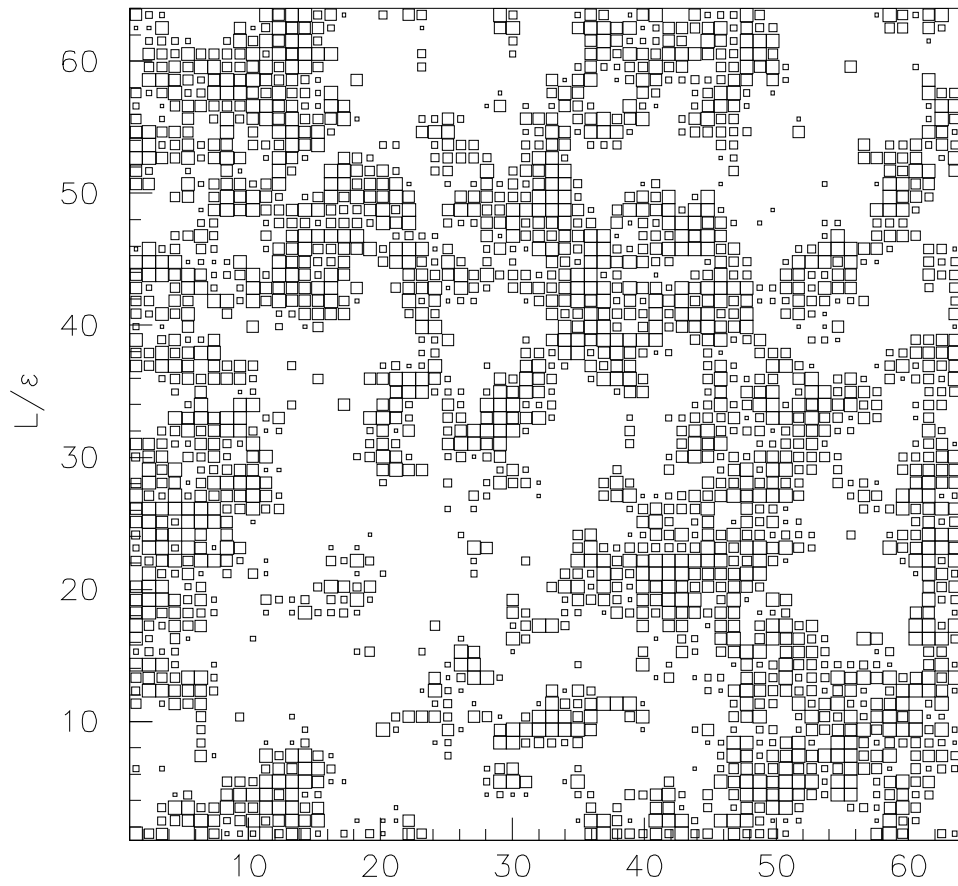


Fig. 2

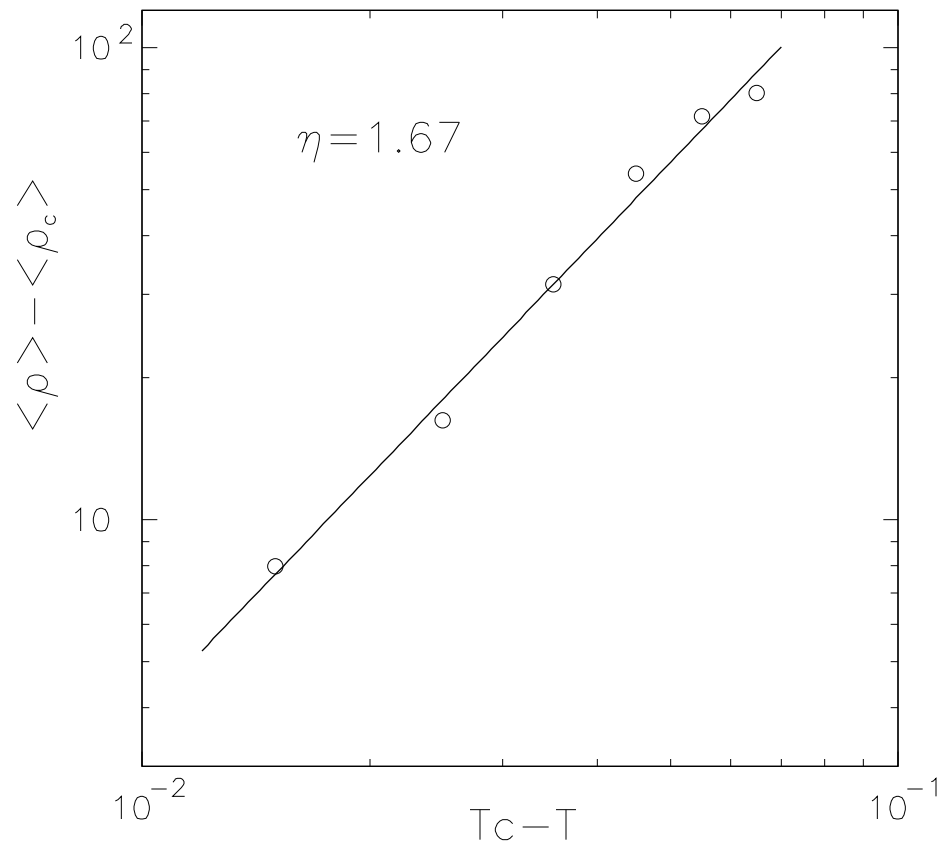


Fig. 3

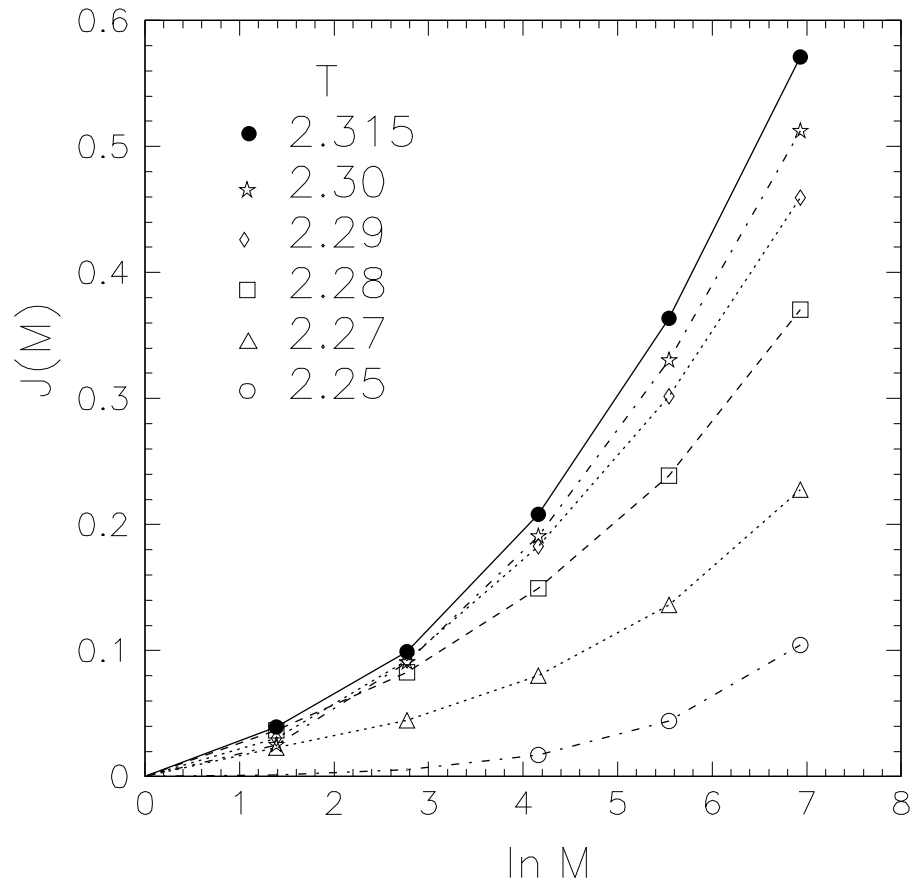


Fig. 4

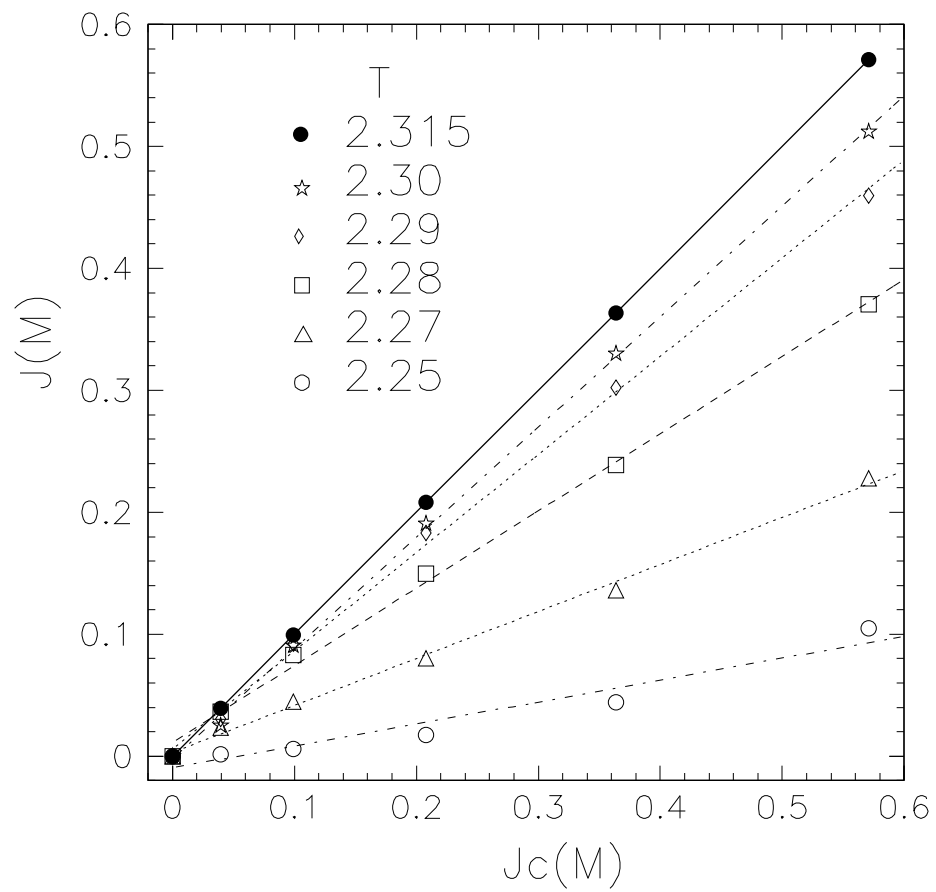


Fig. 5

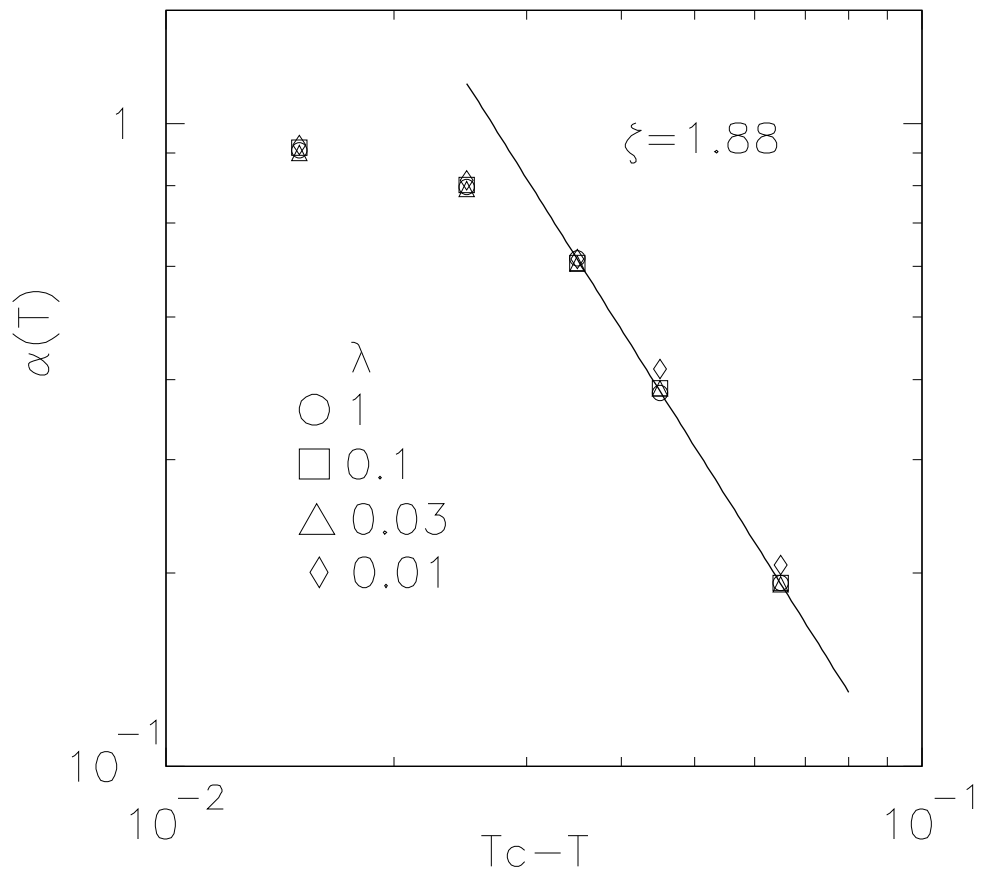


Fig. 6

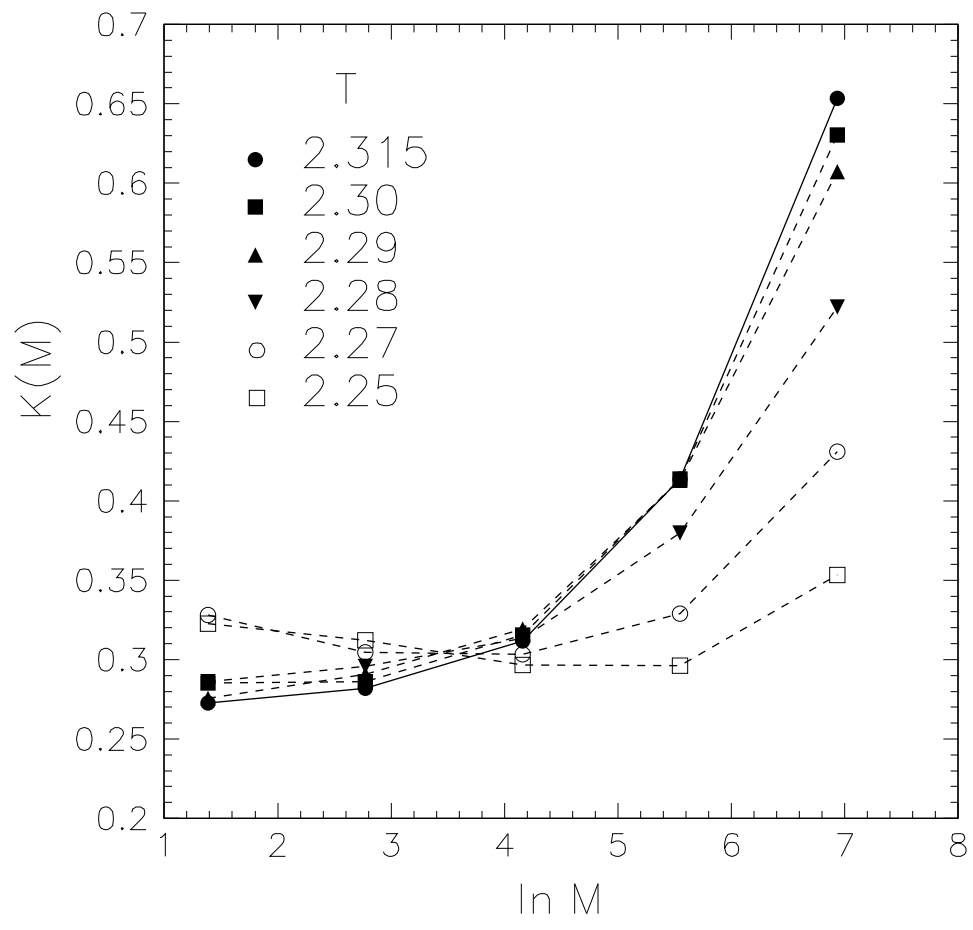


Fig. 7

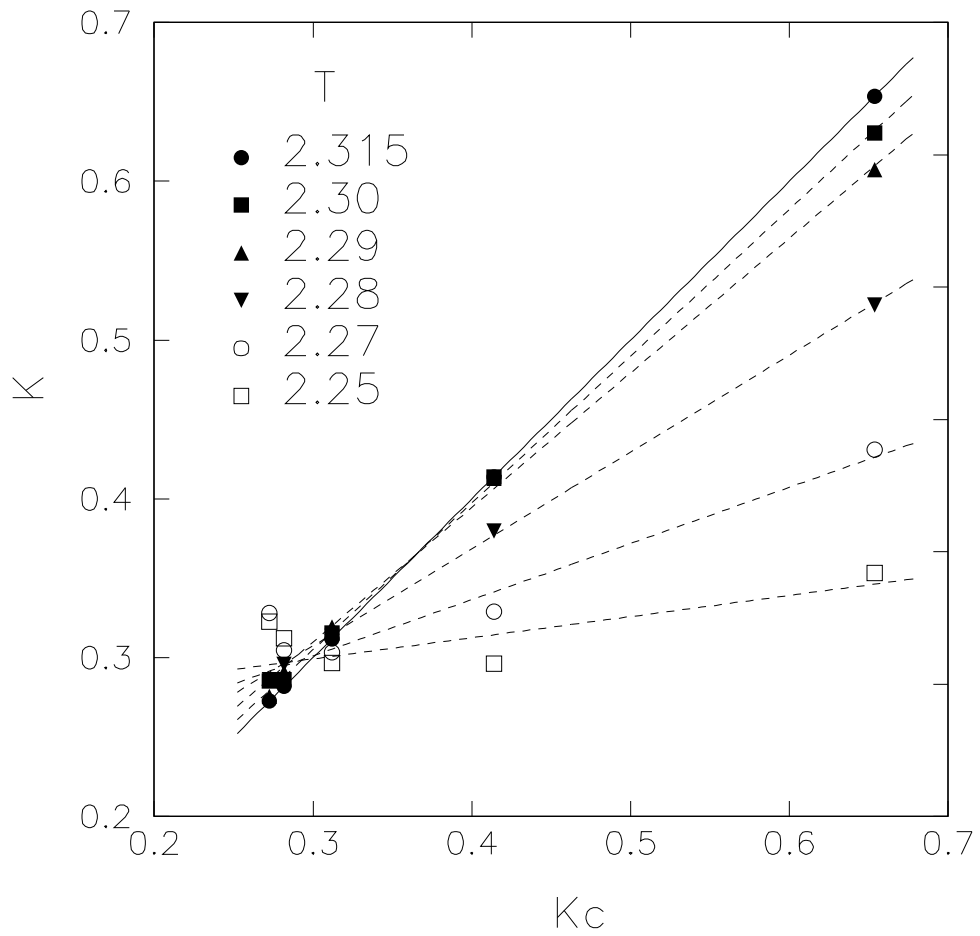


Fig. 8

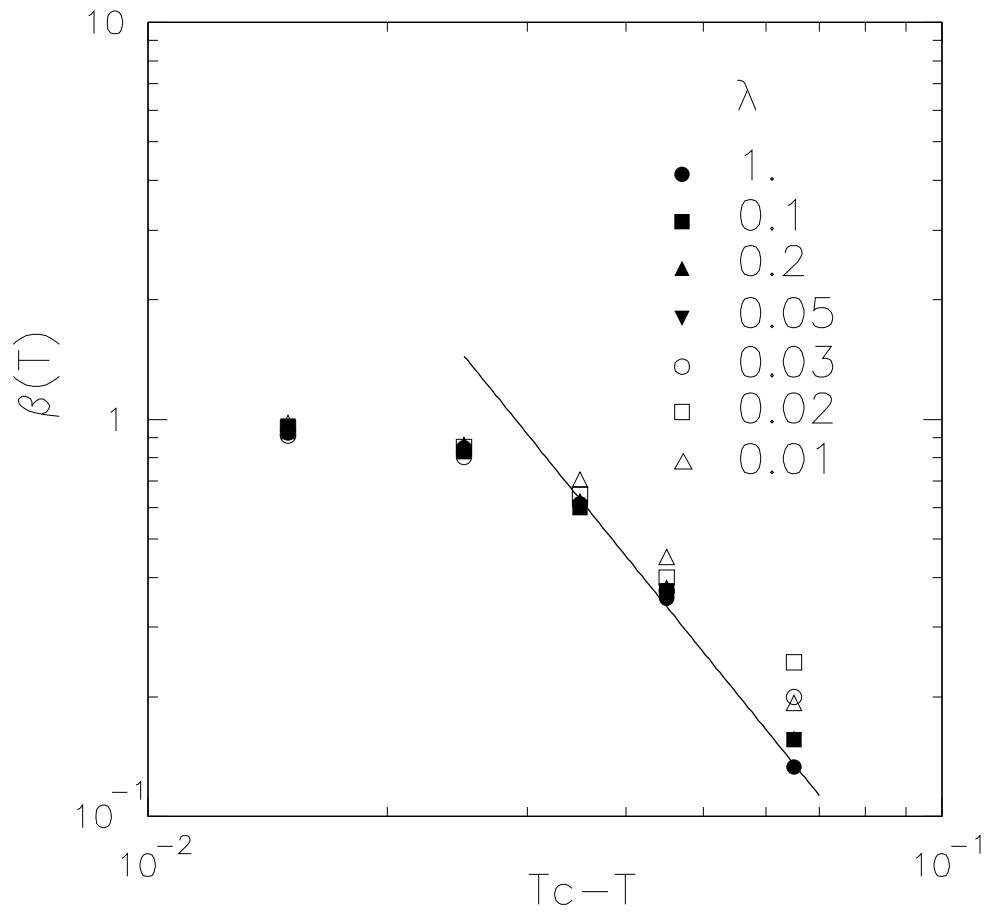


Fig. 9

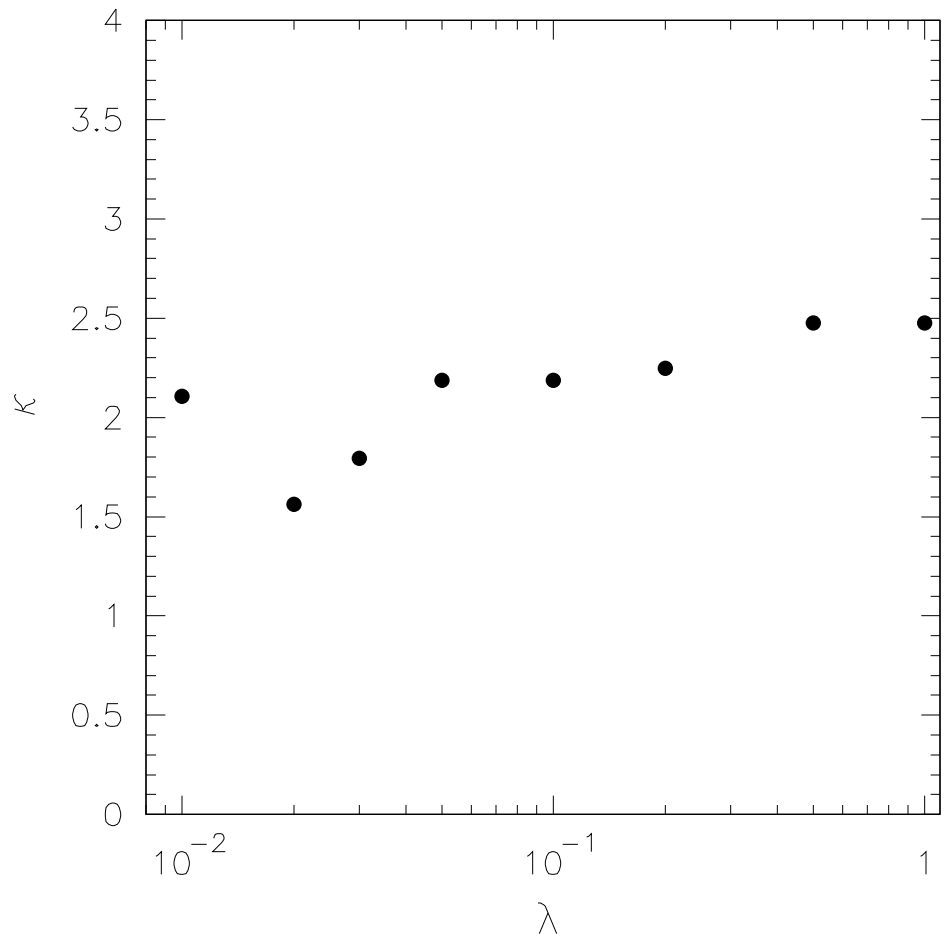
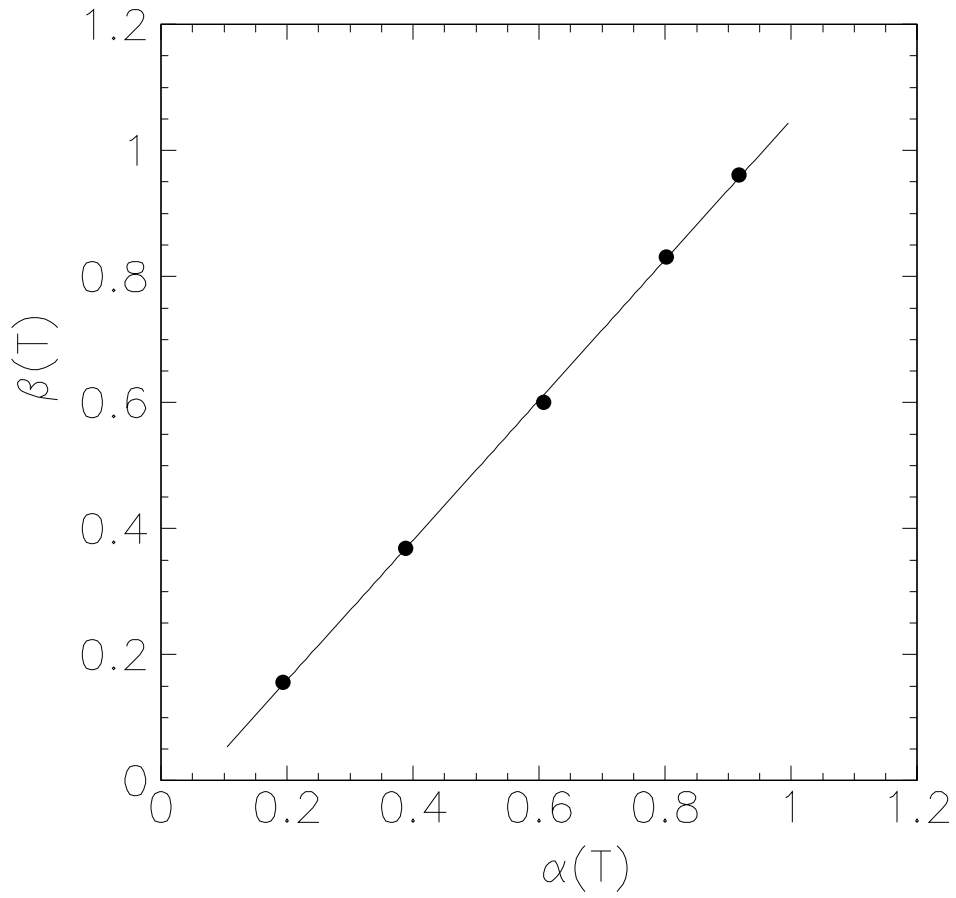


Fig. 10



$\alpha(T)$
Fig. 11

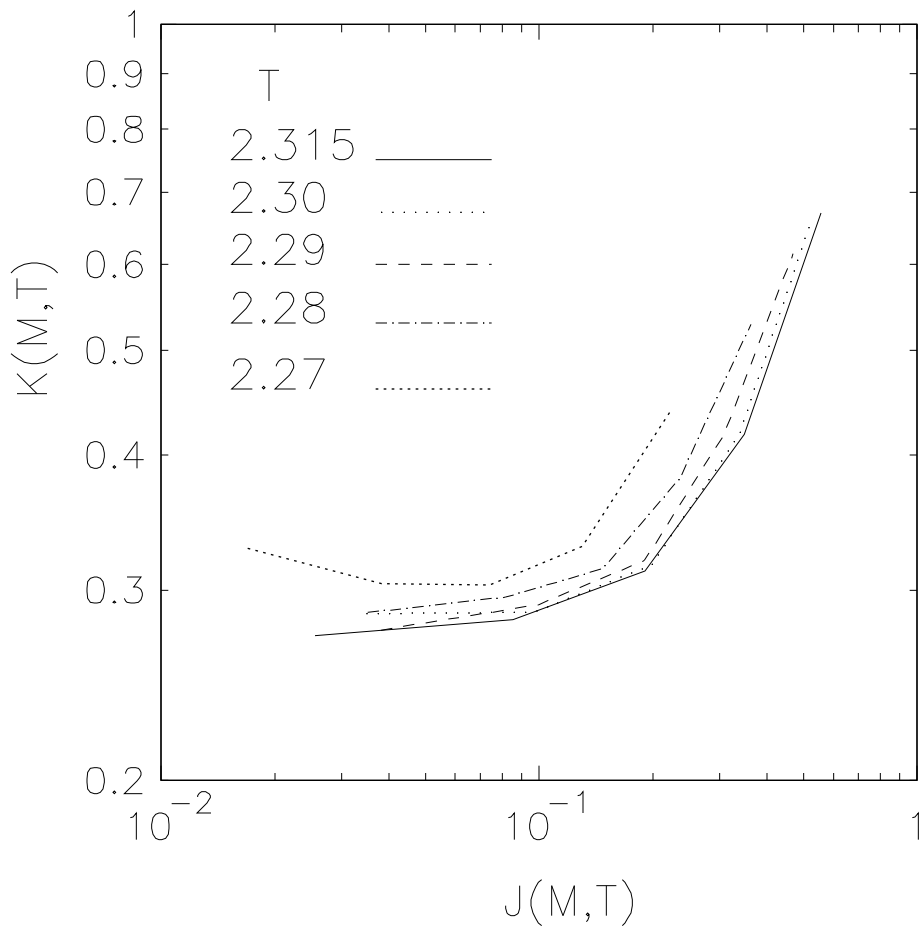


Fig. 12

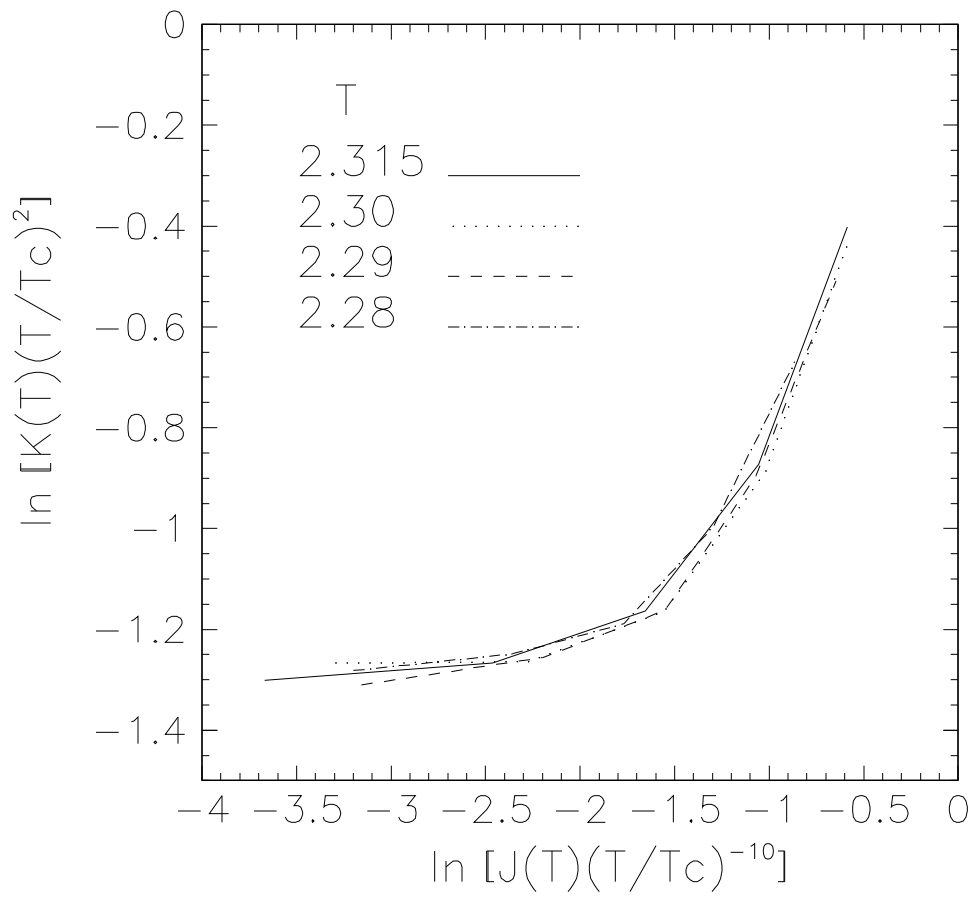


Fig. 13

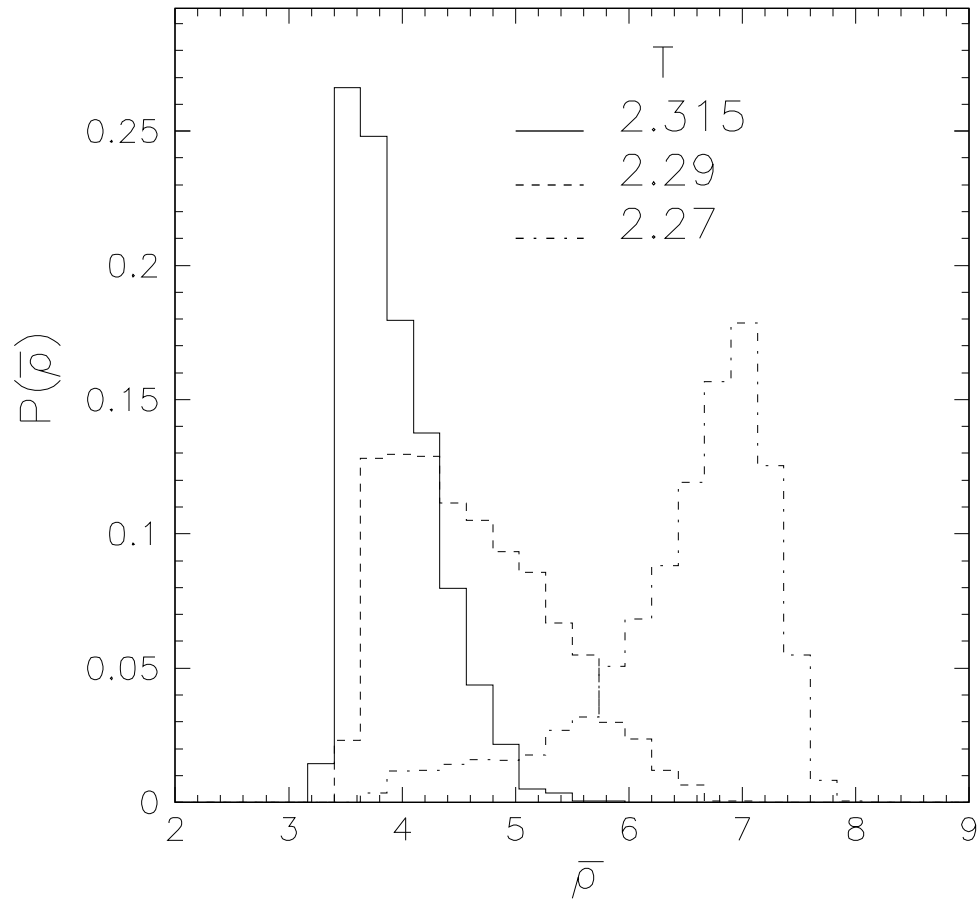


Fig.14

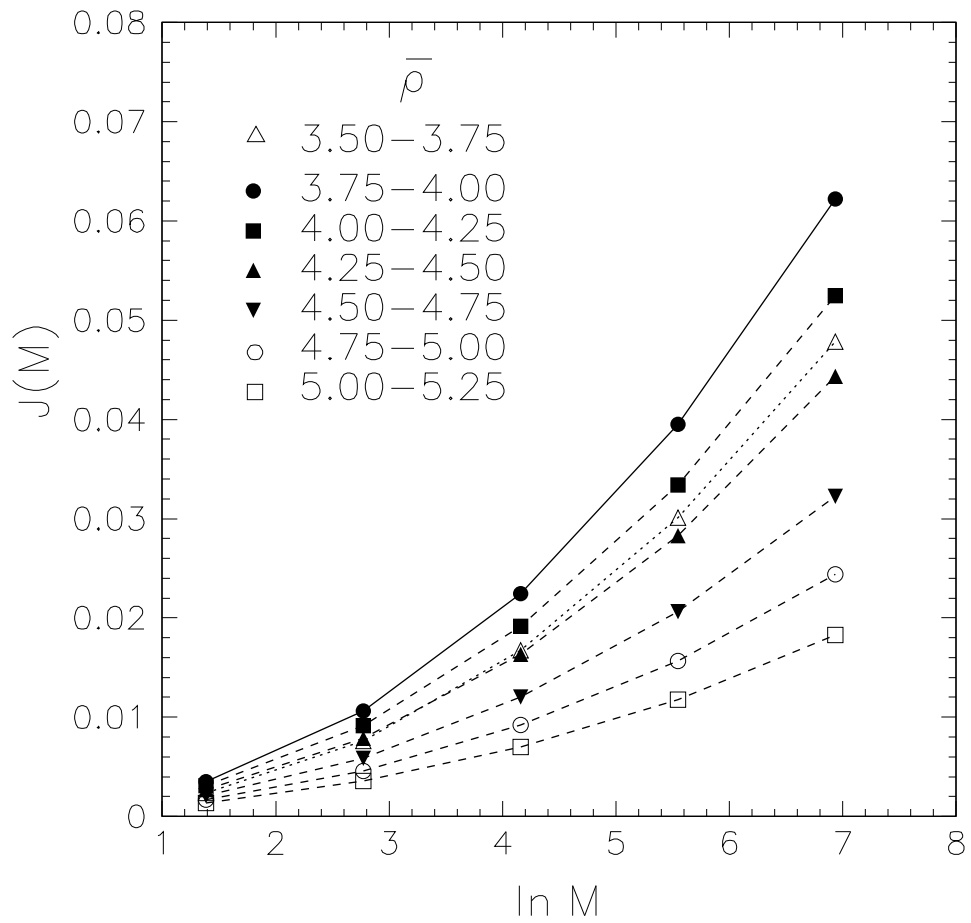


Fig. 15

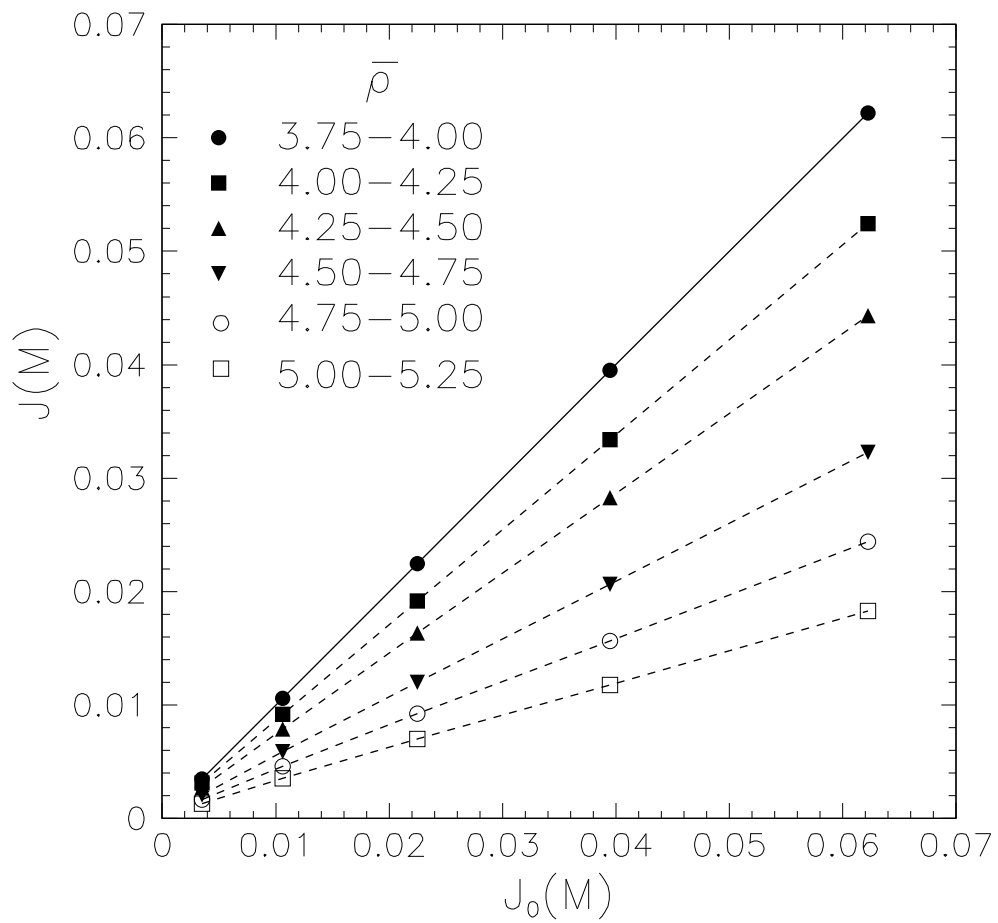


Fig. 16

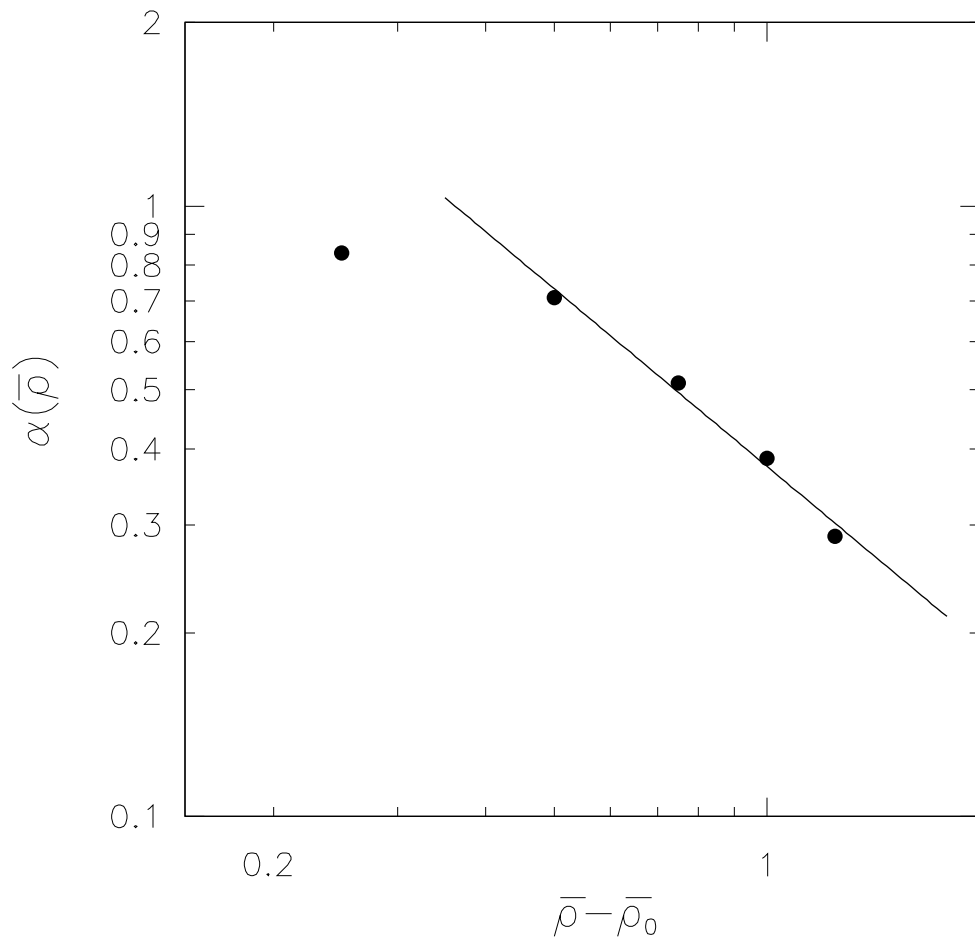


Fig. 17

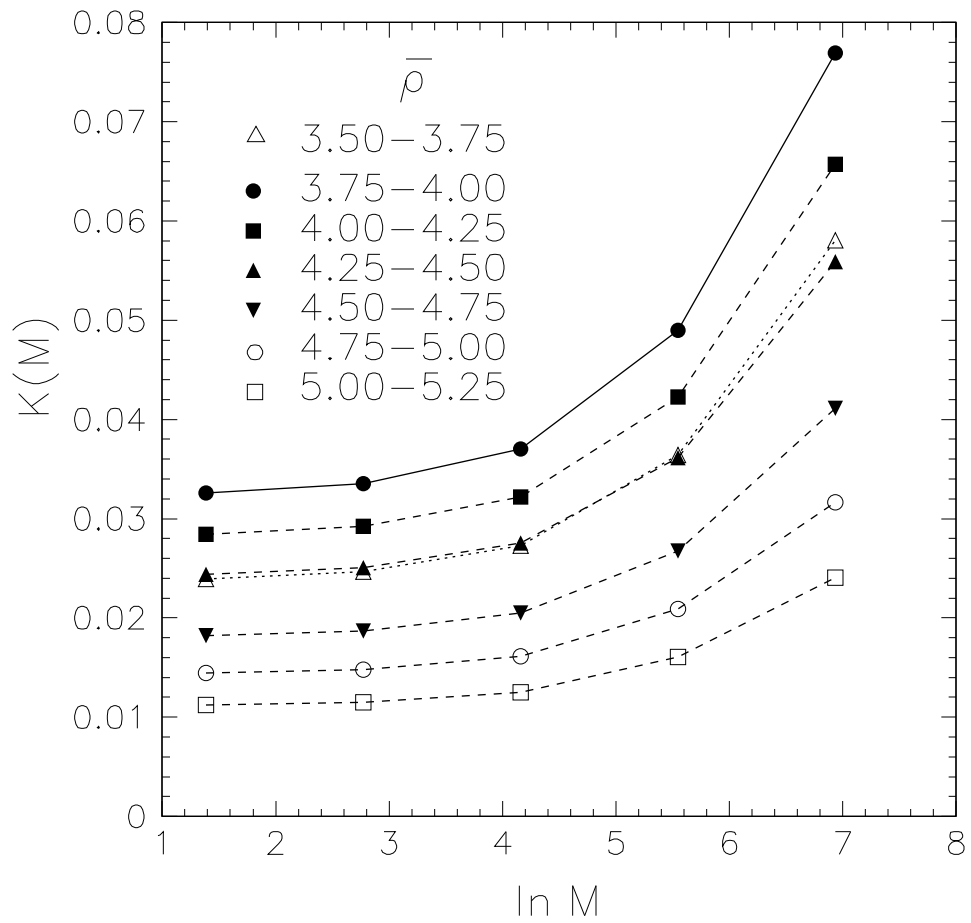


Fig. 18

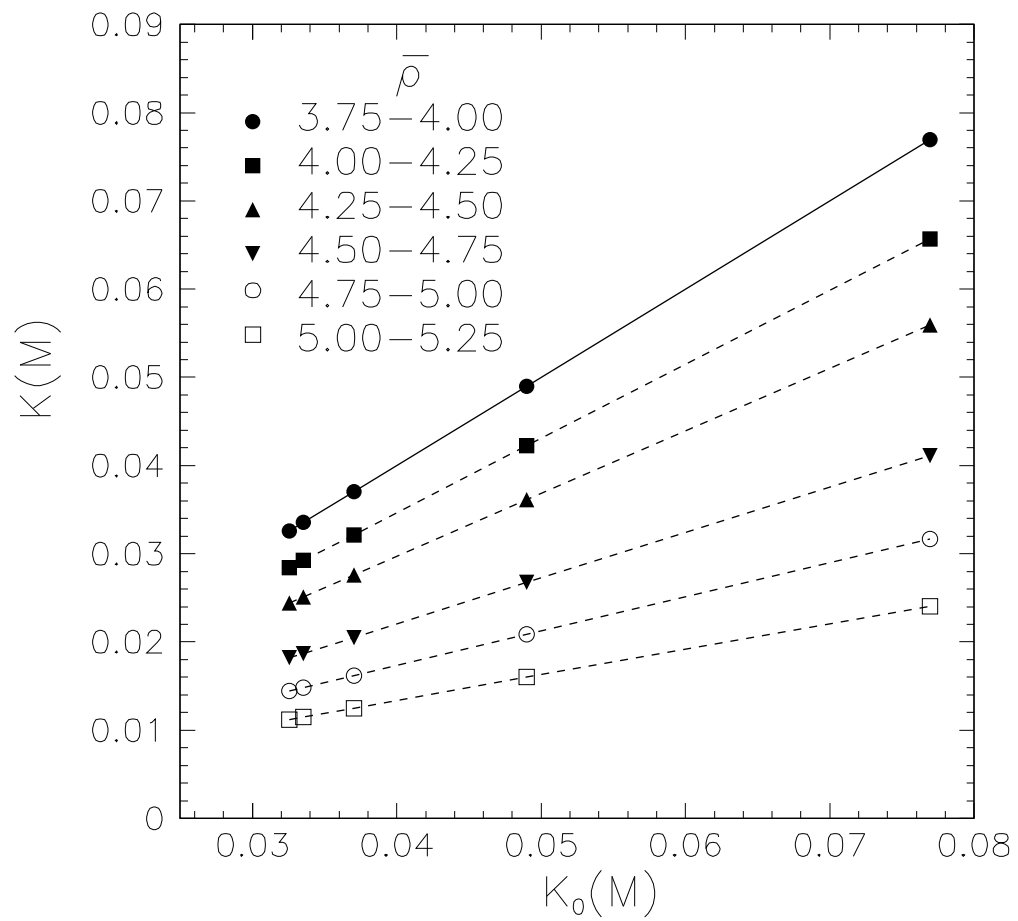


Fig. 19

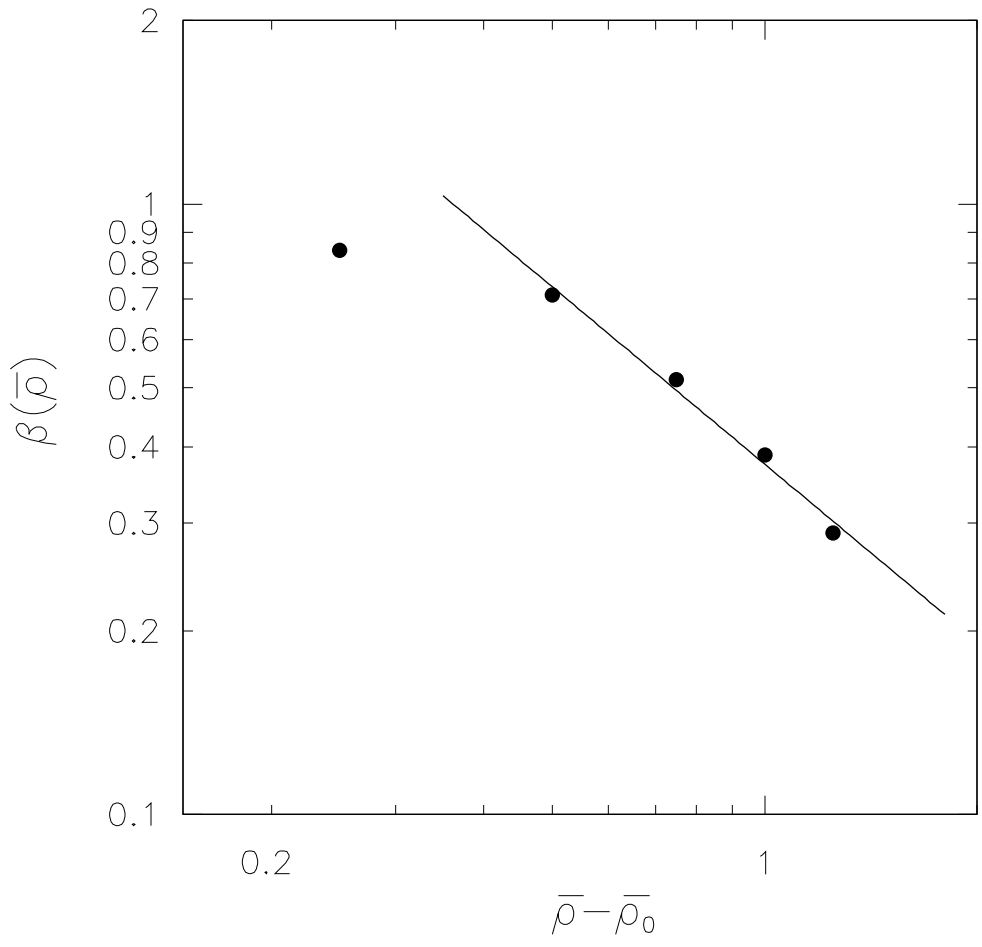


Fig. 20

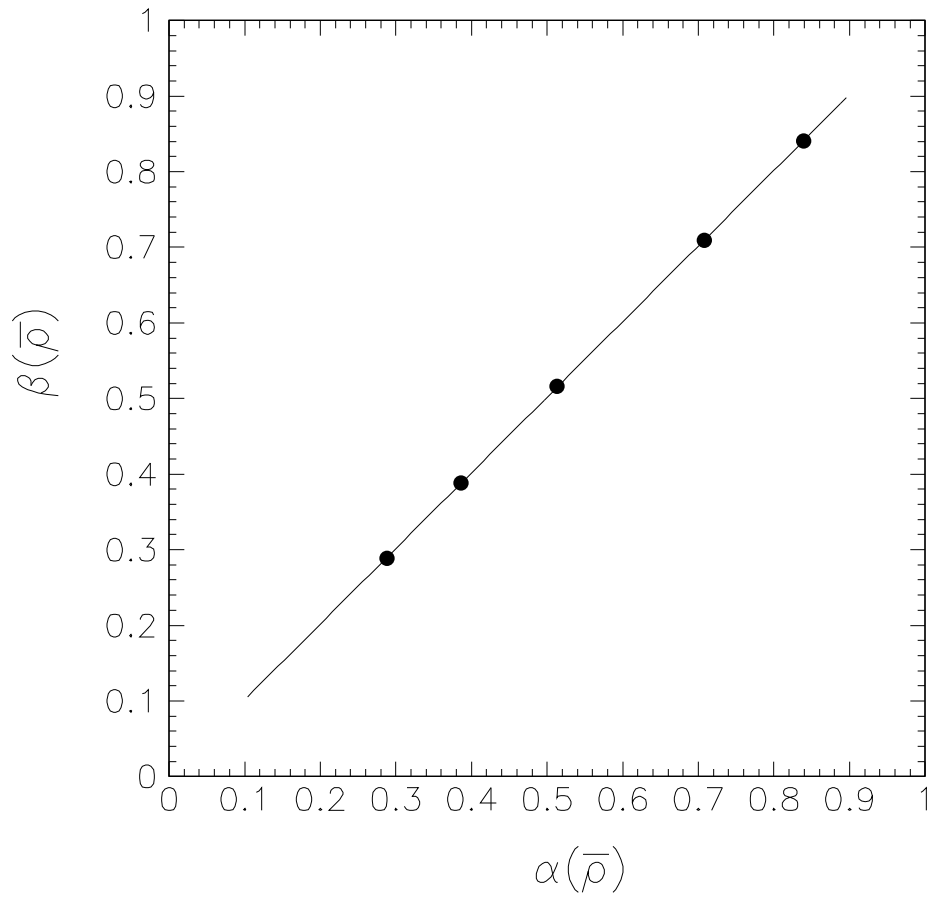


Fig. 21

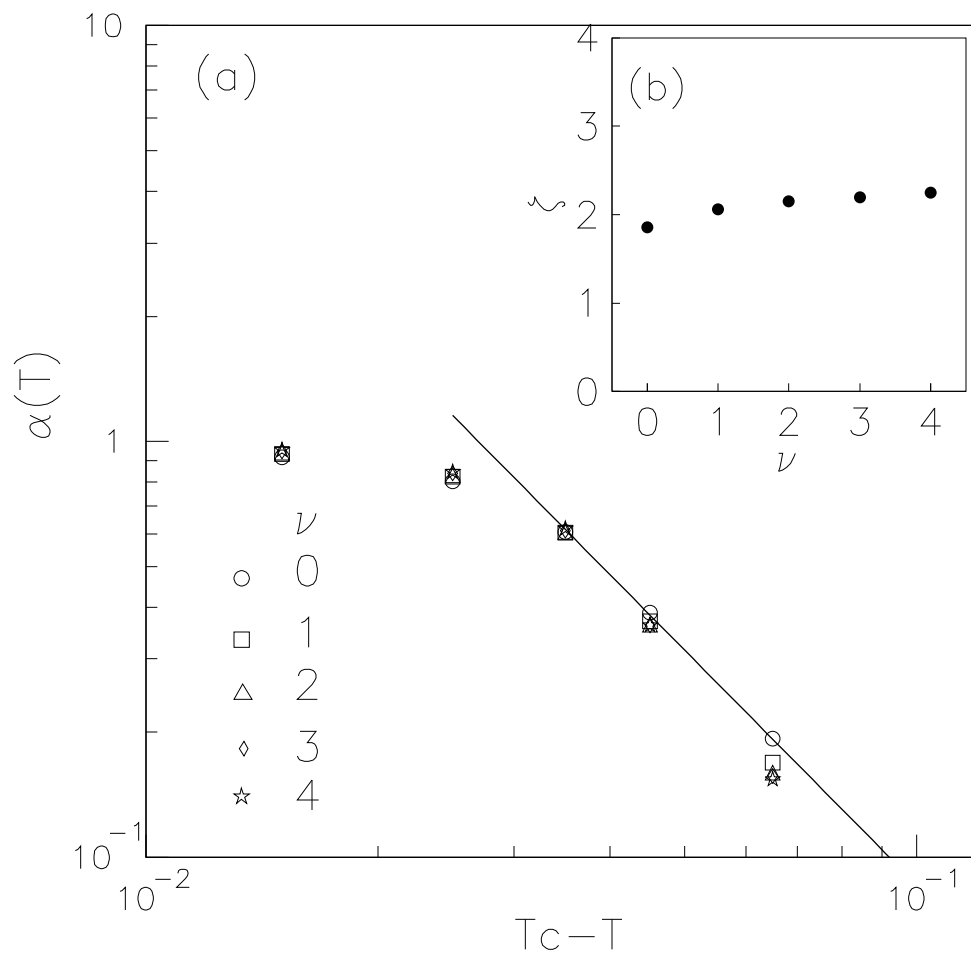


Fig. 22

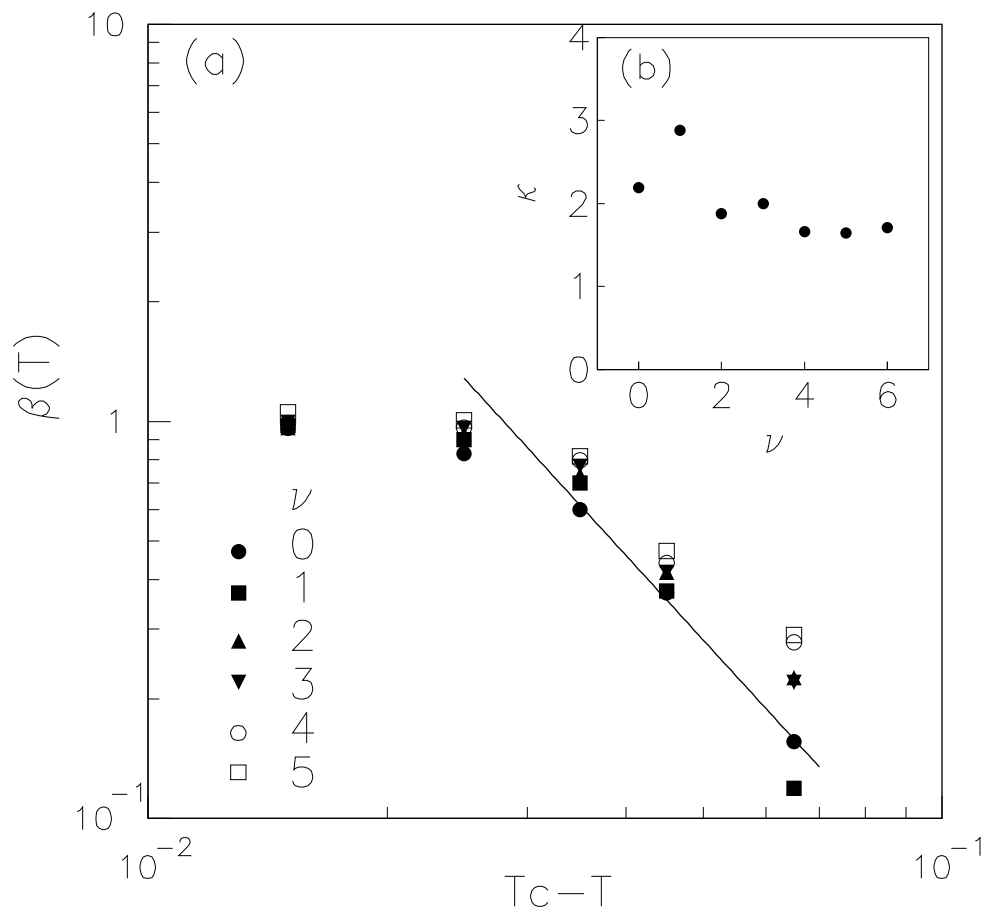


Fig. 23

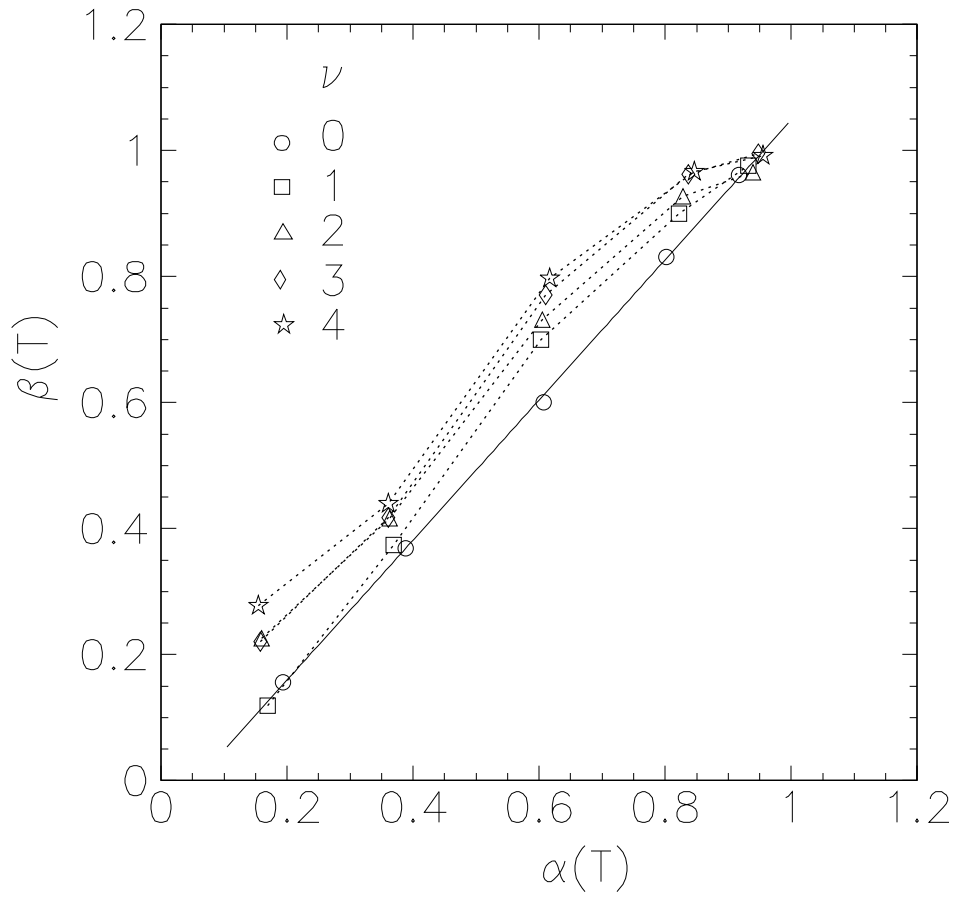


Fig. 24